KEY REFERENCES

-At the start of the manuscript, please highlight up to 5 key references from your lab (including DOIs) that demonstrate the development/use of the protocol. This will be used in the related links section.
- We can also highlight 1 or more of these particular references in the 'associated links' box on the online article page if they are published in Springer Nature journals.
-You can categorize references as suitable to be listed as either 'Key reference(s) using this protocol' or containing 'Key data used in this protocol (Optional heading)

EDITORIAL SUMMARY

-We use short summaries (up to 250 characters) to highlight all our protocols on our home page. This will be used to summarize your protocol on our homepage. Please check this summary is accurate.

A set of procedures for standardising the evaluation of multiphoton microscopes, covering laser power, pulse width optimisations, field of view, resolution, and photomultiplier tube performance.

PROPOSED TWEET

Please feel free to make suggestions, to include your own twitter handles or hashtags. Max. character count = 120.

A set of procedures for standardising the evaluation and optimisation of multiphoton microscopes.

PROPOSED TEASER

This a short (<50 characters) description of the protocol for our website and/or cover. Please check this is accurate.

Evaluating multiphoton microscope performance.

KEY POINTS

2 Key points, with a total length of 70 words (written by the editor and, in the online version of the article, presented after the Abstract and before the Introduction).

- the first is a summary of techniques involved.
- the second is an outline of advantages over alternatives.

TITLE

Standardised Measurements for Monitoring and Comparing Multiphoton Microscope Systems

AUTHORSAUTHORS

Robert M. Lees[1], Isaac H. Bianco[2], Robert A.A. Campbell[3], Natalia Orlova[4], Darcy S. Peterka[5], Bruno Pichler[6], Spencer LaVere Smith[7], Dimitri Yatsenko[8], Che-Hang Yu[7], Adam M. Packer[9*]

[1]Science and Technology Facilities Council, Octopus imaging facility, Research Complex at Harwell, Harwell Campus, Oxfordshire, UK
[2]Department of Neuroscience, Physiology & Pharmacology, University College London, UK
[3]Sainsbury Wellcome Centre, University College London, UK
[4]Allen Institute, Seattle, USA
[5]Mortimer B. Zuckerman Mind Brain Behavior Institute, Columbia University, New York, NY 10027, USA
[6]Independent NeuroScience Services INSS Ltd, Lewes, East Sussex, UK
[7]Department of Electrical and Computer Engineering, University of California Santa Barbara, USA
[8]DataJoint Inc., Houston, TX
[9]Department of Physiology, Anatomy, and Genetics, University of Oxford, Oxford, UK
[*]Corresponding author

Email address for corresponding author: adampacker@gmail.com

KEYWORDS

Multiphoton, microscope, fluorescence, characterisation, comparison, measurement, tools, spatial resolution, laser, power, pulse width, homogeneity, performance, detector

ABSTRACT

The goal of this protocol is to enable better characterisation of multiphoton microscopy hardware across a large user base. The scope of this protocol is purposefully limited to focus on hardware, touching on software and data analysis routines only where relevant. The intended audiences are scientists using and building multiphoton microscopes in their laboratories. The goal of this protocol is that any scientist, not only those with optical expertise, can test whether their multiphoton microscope is performing well and producing consistent data over the lifetime of their system. Individual procedures are designed to take one to two hours to complete without the use of expensive equipment.

INTRODUCTION

Multiphoton excitation was originally described in 1932[1] and the first scanning multiphoton microscope demonstrated in 1990[2]. Since then, the technology has been driven by the use of multiphoton microscopy for imaging deep into scattering tissues. Many research labs now use either custom-built multiphoton microscopes or instruments from commercial manufacturers. However, there are very few accessible tools and procedures for quantifying a multiphoton microscope's performance. This quantification is essential for maintaining imaging performance over time, comparing instruments, and rigorously reporting experimental methods to enable reproducibility.

We think protocols that quantify microscope system performance are necessary for several reasons. First, as developers, early adopters, builders, users, and facility managers, we have realised that there is not always a consensus on which metrics are needed, nor agreement on best practices when performing the relevant measurements. We want to share practices that we think provide the most crucial measurements both efficiently and accurately. Such measurements can provide valuable diagnostic information about system performance, especially when characterisation is performed regularly. Second, we aim to further push the transition of multiphoton microscopy from a frontier technology to a routine tool. Third, we hope this effort will contribute to more reliable comparisons of results within and across laboratories. Fourth, and finally, we aspire to engage manufacturers to specify their microscopes' performance in similarly quantitative ways and develop better tools for such characterisation. Overall, we desire to push the field to improve data quality and rigour for the purposes of efficiency, open science, and reproducibility.

OVERVIEW OF THE PROCEDURES

Many of the procedures in this protocol can be performed independently, but some need to be performed before others in the first instance. Guidance on testing frequency is provided in the anticipated results section. We provide procedures to characterise both the excitation and collection sub-systems of the microscope (**Fig. 1**). For excitation, we cover how to carefully and simply quantify the laser power on sample, the excitation volume (i.e. point spread function; PSF), the field of view (FOV) size and homogeneity, and a protocol for optimising excitation laser pulse width on sample. For collection, we provide a method for monitoring the sensitivity of photomultiplier tubes (PMTs), as well as one for quantifying the photon transfer function of the complete microscope system.

All procedures assume that the reader has all the components needed for a multiphoton microscope, and that they are already configured correctly and controlled by software. While more detailed characterizations can be made with specialised (and expensive) equipment, we designed the procedures to require relatively simple, inexpensive and readily available resources.

LASER POWER AT THE SAMPLE

Measuring and monitoring laser power at the sample is critical in multiphoton microscopy for maintaining sample integrity and data quality. Firstly, emitted fluorescence, often the signal of interest,

is proportional to the average laser power squared, so small changes in laser power can result in large changes to your data. Secondly, exposing your sample to significant laser power can cause photo-bleaching and photo-damage, altering your sample and measurements. Broadly, there are two types of laser-induced photo-damage that can occur in multiphoton microscopy[3]. The first is local heating of the area being imaged, which is linearly related to the average laser power. While this effect may be minor for normal imaging conditions, it should not be ignored, as it has been shown to alter the nature of biological samples[4–9]. The second type of photo-damage is photochemical degradation, such as bleaching or even ablation, which is nonlinearly related to the average laser power[3,10,11]. Therefore, knowing the laser power is essential for consistency between experiments, for minimising or eliminating photo-damage, and for monitoring the health of your imaging system.

Before reaching the microscope scan head, the laser beam is routed through a user-controlled variable power modulator (e.g. a Pockels cell, motorised half-wave plate or acousto-optic modulator). The modulator may be a device that is integrated into the laser enclosure itself or a device that intercepts the laser beam path after it exits the enclosure. Attenuators typically use polarisation or diffraction to send a defined proportion of the beam into a “dump” to safely absorb excess light, whilst the remainder passes through the optical system and reaches the sample. When the user “changes laser power” they are often altering the ratio of power going to the dump versus the sample.

Uncalibrated control software will usually allow the user to set laser power along an arbitrary scale, such as 0% to 100%. What those values mean exactly will depend on the software itself, but most likely they simply map to the minimum and maximum of an analogue voltage output that is fed to the controller electronics of the power modulator. Some microscope control software allows the user to calibrate the on-screen laser power control such that it is mapped directly in watts (W), removing any nonlinearity introduced by the power modulation hardware. Other software has no facility for calibration and will always display power in arbitrary units. In this protocol, we describe the most generic process, which is to manually generate a table for converting percent power into a value in W.

Microscopes can be configured and controlled in a variety of ways that can affect laser power measurements. There are often substantial losses in laser power as the beam traverses the path towards the sample. For example, it is not unusual for the objective alone to have transmission efficiencies of around 70%[12,13]. For this reason, the laser power sensor is placed after the imaging objective to get the best estimate of power arriving at the sample. Note that laser power measurements will be dependent on the objective used and are only valid for that objective. A different objective will likely have different physical properties, such as anti-reflective coatings, different number of glass elements, and a different back pupil diameter, all of which will affect transmission and therefore laser power at the sample.

There are two ways of measuring the time-averaged laser power under the objective: either with the beam stationary (typically centred in the imaging field of view) or with the beam continuously scanning. When possible, we recommend that measurements are made with a stationary beam or scanning with beam blanking disabled, as both conditions are independent of changes in effective duty cycle of the scanning (e.g. from changes in zoom), and easily comparable across different microscopes and power meters. The effective average power on sample during an experiment (with beam blanking enabled) could also be measured and compared to values derived from the scan parameters and duty cycle (which should be provided in publications) to check they corroborate. We note that what is most critical is to use one method consistently, and accurately report the experimental conditions under which the measurements were made.

FIELD OF VIEW SIZE

In conventional laser scanning systems, the image is created by scanning the focused laser beam over a rectangular area with a set of mechanical scanners that steer the beam in the X (fast) and Y (slow) directions. This scan pattern is known as raster scanning. The beam travels over the rectangular area within the sample, exciting fluorophore molecules along the path of the scan. The resulting fast fluorescence emission (often a few nanoseconds) is detected and integrated over a short duration (the pixel dwell time) to create an intensity value for a single pixel. Consecutive pixels are captured and used to create an image.

The area on the sample covered by the scan is known as the field-of-view (FOV). The maximum area that can be scanned is limited by the optics within the microscope, the objective chosen, and the scanning hardware, but under normal conditions is restricted by controlling the X and Y mirrors' scan angle. This can be changed in software by changing the maximum galvanometer scan amplitude to "zoom in" on some specific structure or "zoom out" to see the maximum FOV. For additional information on the relation of FOV to the hardware parameters, see[14–18]. When using conventional galvanometers, the speed at which the scanners trace a line can be varied by the user, allowing changes in the rate at which lines are scanned. For resonant galvanometers, the period is fixed by the mechanical properties of the scanner, and only scan amplitude can be changed.

Knowing the physical size of the FOV allows the pixel-pitch in microns to be calculated. From this you can measure physical dimensions of features in the imaged sample as well as select the correct zoom factor to achieve spatial sampling that takes advantage of the full optical resolution of the system (known as Nyquist sampling), if required. Furthermore, measuring FOV size is an essential step for characterization of the imaging system: measurements in other procedures of this protocol (e.g. **Procedures 3 and 4**) will rely on an accurately calibrated FOV. Additionally, an uncalibrated system may have non-square pixels, and measuring the pixel size is a prerequisite for correcting this should it be necessary.

FIELD OF VIEW HOMOGENEITY

FOV homogeneity is a metric that defines the system's uniformity of excitation and collection of light across the FOV of the sample. Measuring field homogeneity is easy to do and can be used to understand the data quality across the image, and to know the experimental FOV size that minimises this variation. Large, structured variations in FOV homogeneity can also highlight potential problems with microscope alignment or debris on optics in the path.

One common inhomogeneity that can be revealed from this measurement is known as "vignetting", where signal is reduced at the edges of the FOV. Vignetting is important to consider when choosing the working FOV for experiments as reduced signal at the edges of the FOV will cause a decrease in signal-to-noise in those regions.

Vignetting is unavoidable when using large scan angles that are at the design limit of the microscope hardware and optics. The limits are defined by the optical properties of the microscope, particularly the objective lens. Manufacturers usually specify the FOV size over which an objective's performance is said to be "diffraction-limited". Beyond the specified FOV size, the objective's ability to focus light degrades significantly and causes vignetting and other optical aberrations. Typically the objective is the principle limit for the FOV size, but an improperly designed excitation or collection path might become a limiting factor depending on PMT sensor size, angle of acceptance, and the collecting lenses (for more on this topic, see[19,20]).

SPATIAL RESOLUTION

Laser scanning imaging systems such as multiphoton microscopes provide spatial resolution governed by their point spread function (PSF). The point spread function is the impulse response of an imaging

system. In other words, the PSF describes how a point object (an "impulse") in the object space will be “spread” by the imaging system, and thus appear in the acquired image. The PSF is a three-dimensional spatial function whose shape can vary depending on the focusing optics of a system, and across the field of view. Moreover, nonlinear excitation and excitation saturation can influence the effective spatial resolution in multiphoton microscopy[21]. Thus, in this protocol the excitation volume geometry means the shape of the volume that is excited by the focused laser light at a given point in time. The geometry of the excitation volume governs how the smallest features will appear in the microscope and the effective spatial resolving power of the microscope. In multiphoton imaging the shape of the excitation volume is commonly characterised, often approximated by the full-width at half-maximum of the axial and radial profiles, and that is the procedure we describe in this protocol.

The measurement of an excitation volume matters because it indicates how an imaging system resolves signals from structures in the sample, and the profile of the excitation volume can be engineered depending on the requirement of the application. For common use-cases, the imaging system is designed to achieve a diffraction-limited PSF (the highest resolution possible for a system limited due to the physics of diffraction), which would ideally be smaller than the structures of interest being observed[16,21,22]. In this way, the emission from the excitation volume is dominated by signals from individual structures, and contributions from neighbouring structures are minimal. We note that the term “diffraction-limited” is typically applied to beams with planar or gaussian wavefronts that then enter and are focused by standard objectives. In contrast, there are purposefully designed non-diffraction-limited PSFs, which match or are much larger than the structure of interest, these are utilised to rapidly sample volumes of tissue, especially when staining is bright and sparse[23–28]. Regardless of the experimental approach, excitation volume geometry should be characterised and monitored over time to ensure consistent resolution within a set of experiments. Although the example shown in this protocol is the diffraction-limited case, this protocol is empirical and applies in non-diffraction-limited cases as well.

The numerical aperture (NA) is a unitless parameter that characterises the range of ray angles that an optical system can accept or emit. The NA and wavelength of the excitation light are the major factors that influence the smallest possible spatial extent of the PSF, such that larger NAs and shorter wavelengths lead to smaller PSFs. The maximum possible NA is set by the objective. However, if the excitation light entering the objective underfills the back pupil, then the effective excitation NA will be reduced and the actual PSF is larger than the theoretical, diffraction-limited prediction for that objective[29,30]. The profile of the beam used to illuminate the back aperture is approximately Gaussian in most cases, and its width is commonly characterised by the spatial extent over which the intensity exceeds $1/e^2$ of its maximum (e is the base of the natural logarithm). Thus, to use the full NA of the objective the back pupil of the objective must be overfilled, leading to some power being discarded. Sometimes objectives are deliberately underfilled to transmit more power, or for application-specific PSF engineering strategies; other times underfilling is unintentional and due to clipping or limiting apertures in the microscope optical path. In either case, the excitation volume will have a larger spatial extent than predicted by theory for the objective’s listed NA.

Besides the NA and wavelength, other experimental and sample specific factors affect the resolution. For example, the refractive index (RI) varies for materials. Air has an RI close to 1, water has an RI around 1.33, and different types of glass can exhibit RIs in the range from about 1.5 to 1.9. When light rays are converging to a focus, discontinuities or changes in the RI can cause marginal rays to be refracted more strongly than rays close to the optical axis, thus degrading the quality of the focus. This condition is a type of optical aberration called spherical aberration (SA), and SA will reduce the actual spatial resolution from the theoretical prediction. This resolution degradation is typically more pronounced in the axial direction, the direction along which PSFs often have their longest spatial extent. SA can be reduced by matching the RIs of the immersion medium and the sample, when possible. Some microscope objectives correct for some SA through compensation mechanisms such as a correction collar, which can restore diffraction-limited imaging over a range of RI mismatches. In other systems adaptive optics such as deformable mirrors can compensate for such aberrations[31,32]. Although SA could be corrected, RI mismatch also gives rise to a different focal shift for the imaging plane from the travelling distance of the stage (or the objective) along the z-axis (Fig 2). This unequal displacement results in axially distorted images, either compressed

or elongated. A correction factor can be calculated to correct for this axial distortion and should be applied[33,34].

Overall, off-axis aberrations intrinsic to the lenses (e.g. coma and astigmatism) gradually increase and deteriorate the geometry of the excitation volume toward the periphery of the FOV. The aberrations are the result of the combination of relay optics, objectives, the arrangement of scanners (closely coupled or separately-conjugated orthogonal scanners), and so on. Measuring the resolution across the FOV is recommended, especially for a large FOV (>1 mm) imaging system.

It is worth noting that tissue scattering deteriorates the resolution in a depth-dependent manner, as the marginal rays out of the objective travel a longer distance than an on-axis ray and accumulate larger scattering and attenuation. The difference in travelling distance can result in a smaller effective NA and impacts the effective excitation volume as the imaging plane goes deeper, especially for high NA objectives[35,36]. This resultant degradation in signal and resolution can be more severe than simply starting with a lower effective NA, and is a reason why it is generally recommended to underfill objectives when imaging deep[37,38].

Note that the excitation volume measured in this protocol is focused on characterising the imaging system only. Imaging biological specimens will entail additional aberrations and scattering, which can be compensated for by adaptive optics[39].

PULSE WIDTH CONTROL AND OPTIMISATION

Nearly all multiphoton microscopy makes use of modelocked[40] ultrafast lasers with pulse durations on the order of 100 femtoseconds (100 x 10^{-15} seconds). Due to the non-linearity of multi-photon excitation, peak intensity matters more than average power for efficient excitation. The efficiency of multi-photon excitation using pulsed lasers versus CW (continuous wave) lasers, with the same time-averaged power, is given by:

$$g^{(n)} = \frac{g_p^{(n)}}{(\tau f_R)^{n-1}} \quad \text{(eq. 1)}$$

where $g^{(n)}$ = enhancement factor, τ = pulse width, f_R = repetition rate, n = number of photons in the absorption process[16]. The factor $g_p^{(n)}$depends only on the pulse shape, and is equal to one for a rectangular pulse and 0.59 for a hyperbolic secant ($sech^2$) envelope, which is close to the typical shape of the pulses delivered from modelocked pulsed lasers[40]. For two-photon imaging, with a standard Ti-Sapphire laser operating at 80 MHz with 150 femtosecond pulses, this enhancement over CW lasers is ~50,000, and is strongly dependent on τ, the pulse width.

The generation of short laser pulses requires finite bandwidth - the shorter the desired laser pulse, the broader the spectral content. This can be rigorously derived classically through Fourier transform relationships, and for the $sech^2$ envelope mentioned above, leads to $\tau_p \times \Delta v_p \geq\geq 0.3148$, with $\tau_p$the full-width at half-maximum (FWHM) of the laser pulse envelope, and $\Delta v_p$the FWHM of the frequency spectrum[40]. Converting frequency to wavelength means a 150 fs pulse centred at 920 nm needs at least a FWHM bandwidth of 6 nm, a 100 fs pulse 9 nm, and a 50 fs pulse 18 nm. It is important to note that broad bandwidth alone does not *guarantee* a short pulse, but is *required* to generate one. When the pulse is the shortest it can possibly be, given the nominal bandwidth envelope, the pulses are known as *transform-limited pulses*.

Once a transform-limited pulse leaves the laser, the pulse envelope and spectral phase can often be altered through interactions with materials that introduce dispersion, like optical glasses. A dispersive material is one that has a frequency (wavelength) dependent refractive index. If the refractive index increases with increasing frequencies (decreasing wavelength) the material is said to have positive

dispersion, whereas if the refractive index decreases with increasing frequency it is said to have negative dispersion. At the common wavelengths used in microscopy, most materials exhibit positive dispersion[41]. The refractive index can be related to the speed at which light travels through a medium; for positively dispersive media, the bluer portion of the pulse travels at a slower velocity than the redder portion, temporally broadening or "stretching" the pulse, and resulting in a "chirped" pulse. If there is a material with negative dispersion, the opposite occurs, the redder part of the pulse is delayed relative to the bluer. For a given material, the more material that the pulse propagates through, the greater the temporal broadening or stretching. Microscopes with elaborate optical systems (such as large FOV systems[42]) have more or thicker glass elements, as most glass lenses introduce only positive dispersion, the results are additive and can become significant. Similarly, head-mounted multi-photon systems that require a long fibre optic cable for beam delivery will generate a lot of dispersion (unless specialised fibres are used)[43,44].

The broadening effect can be counteracted with a process called dispersion compensation, where the user purposefully introduces a fixed magnitude of dispersion that exactly matches that of the microscope's optical path, but of the opposite sign, such that the combined dispersion from the compensation unit and microscope sums to zero net dispersion. Some lasers have dispersion compensation included as an integral component option (e.g. Coherent Vision and Axon, Spectra Physics Mai-Tai DeepSee and others). For lasers that do not include dispersion compensation, either a commercial or home-built external dispersion compensation unit is used, or in many cases, no compensation system is present, and the user has limited opportunity to modify the pulse width, but should still consider the role dispersion may play in their system.

For two-photon microscopy, the main consequence of temporally stretched pulses is that the effective two-photon excitation efficiency drops. The drop in efficiency for non-linear processes is often significant, even though the total average power being delivered to the sample remains the same. For higher order processes, such as three-photon excitation, the fall-off in signal with longer pulse widths is even more rapid. For shorter pulses (<=50 fs) it is especially important to note that the complete "dispersion" relationship also includes higher order terms that may need to be controlled as well[45,46].

PHOTOMULTIPLIER TUBE PERFORMANCE

Most multiphoton microscopes use one or more photomultiplier tubes (PMTs) to detect light. In brief, the objective and collection optics direct photons emitted from the sample to the primary photosensitive element of the PMT, its photocathode. Photons having sufficient energy will cause a photoelectron to be generated via the photoelectric effect and then amplified through a cascade of dynodes (involving a high potential difference distributed across a chain of increasingly positive dynodes). This converts single photoelectrons to a much larger number of electrons at the PMT anode (roughly 10,000 to 100,000). The bolus of charge arrives at the anode over ~5-10 ns yielding a small burst of current. Typically, a transimpedance amplifier (TIA) is then used to convert this photocurrent to an analogue voltage and amplify that further. That voltage signal is then digitised by a high-speed analogue to digital converter (ADC) card in the acquisition system.

It is important to acknowledge that PMT performance, particularly for the more sensitive GaAsP detectors, degrades over time. Therefore, the PMT should ultimately be regarded as "consumable" and be replaced periodically if the microscope's detection performance is to be maintained. Most often, degradation is related to the total charge that has passed through the PMT, and this leads to a loss of both cathode sensitivity and photocurrent amplification but can also manifest as an increase in dark current and a decrease in dielectric resistance[47]. Moreover, "day one" performance, as well as rate of decline, vary substantially across units of the same PMT model and the rate of deterioration is influenced by usage (for example light exposure and average anode current).

A quantitative means to characterise PMT performance is therefore useful to (1) select between

different units when installing a new PMT into the microscope, (2) diagnose issues that might arise with image quality and (3) benchmark performance over time to make informed decisions about when to replace a PMT.

We note that a lab's specific performance requirements and financial considerations will also play into decisions around when to replace PMTs. However, by quantifying performance, a consistent policy can be adopted that, alongside other routine tests and maintenance described in this protocol, should allow minimum standards of data acquisition to be maintained.

ESTIMATING ABSOLUTE MAGNITUDES OF FLUORESCENCE SIGNALS

The overall acquired fluorescence signals are influenced by factors such as laser power, focus, properties of the fluorescent indicator, light scatter, and overall detection efficiency. It is imperative to understand and control each factor. Mismanagement of any of these factors can lead to a substantial decrease in signal intensity.

Fluorescence signals are commonly expressed in arbitrary units or on relative scales, such as the dF/F ratio (the amplitude of fluorescence change relative to the baseline fluorescence level), masking any degradation in signal magnitude. As a result, two laboratories following similar imaging protocols may record vastly different signal strengths for similar measurements, such as somatic calcium signals, without realising the discrepancy. Low signal magnitudes lead to noisier, less precise measurements. However, without a method to evaluate quantitative signal magnitudes that could allow a lab to detect and address imaging system problems, labs may instead attempt to only compensate for decreased magnitudes of signals through post processing, missing opportunities for improving the primary data.

We suggest reporting fluorescence signals in absolute physical units such as detected photon counts per second—instead or in addition to simply reporting the relative dF/F signal. This standardised method offers a consistent and clear way to demonstrate signal levels, making it an invaluable tool for longitudinal system performance monitoring and simplifying comparisons between different imaging systems.

Direct photon counting, while feasible, is currently rare in multiphoton microscopy, as it requires specialised electronics[48]. However, it is possible to use signal noise statistics to accurately estimate the detector *photon sensitivity* and translate detected signals into estimated photon counts. Photon count estimation is well established in photon-limited imaging modalities such as radiography[49]. Prior multiphoton studies have included variations of this procedure in their analysis[50–52]. However, the method has not yet been applied uniformly across labs to establish quantitative benchmarks. Here we provide a procedure for estimating the photon sensitivity, the photon flux (photon counts per unit area per unit time), and photon rates (e.g. photon counts from an entire cell per unit time). We also provide a guide for interpreting these results. This approach offers a quick and intuitive way to evaluate imaging performance. However, it is important to recognise that it does not provide a detailed understanding of specific problem sources within the system. While the method works best on static fluorescent slides, it can work well even in the presence of physiological signals although care must be taken to recognize and isolate the quantum noise. The consistent application of this absolute metric can lead to universally accepted standards for recorded signal quality, fostering precise expectations and enhancing reproducibility across the scientific community.

ADVANTAGES AND LIMITATIONS

These protocols are intended as a practical resource for the multiphoton imaging community. This is not meant to be an encyclopaedic resource on the theory, design, or complete optical and detection characteristics of the instruments. We are purposefully focusing on measurements that can be performed by

users with turn-key systems, i.e. those without advanced optical metrology equipment. For example, we are not including a procedure for measuring the pulse shape and spectral properties, which would require an expensive optical device (an autocorrelator) as well as significant optical expertise to use it properly. Therefore, this protocol is not a complete characterisation of all aspects of multiphoton microscopy hardware relevant for designing such a system. In short, this is not a 'build' manual as there are already many such excellent resources like[14,15,53–55], as well as many books, articles, and publications that include information more directly relevant to either designers, or to readers interested in historical background or practice[2,14,16–18,21,29,56–61].

We have executed these protocols on many different multiphoton systems and made the step-by-step instructions as generic as possible, however it is still possible that some measurements may be difficult to perform on some systems, depending on software control limitations.

ALTERNATIVE METHODS

Alternative characterisation efforts are underway; for example, the QUAREP-LiMi initiative (https://quarep.org/) that aims to improve quality assessment and quality control for light microscopy. This effort, with widespread community support from scientists and manufacturers, has already produced protocols for general light microscopy[62–64]. Our goals are different in that our narrower focus is meant to provide a single, comprehensive characterisation of a multiphoton microscope.

There are many protocols on various aspects of quality control for confocal microscopes, many of which use similar scanning optics to those used in multiphoton microscopes (PSF only[63,65], quantification[66], reporting[67]). Our effort is also similar to a recent protocol on "Strategic and practical guidelines for successful structured illumination microscopy"[68]. These protocols do not cover key issues specific to the multiphoton case, however see recent publications regarding laser assessment[45,69], as well as earlier multiphoton-centred literature[56,70]. For the nonlinear excitation that enables multiphoton microscopy, pulsed laser sources are required and thus additional factors such as laser pulse repetition rate, pulse width, and compensation for pulse broadening require consideration. Additionally, test samples must undergo efficient two-photon excitation without bleaching or burning, which makes some quantifications particularly challenging. Finally, it is important to characterise multiple aspects in a coherent fashion, so our goal is to have a collection of related procedures in one protocol. The presented methods were chosen by the authors based on cost, ease, and practicality constraints. A detailed review of competing approaches is beyond the scope of this protocol.

MATERIALS

SOFTWARE

- Software that can manipulate images (ImageJ/FIJI, MATLAB, Python/Napari)
- Software that can plot data (MATLAB, Python)
- Microscope control software that allows for live image histogram viewing

EQUIPMENT AND REAGENTS

- Laser scanning multiphoton microscope system
  ▲ **CRITICAL** Keep a shared, dated log of all changes to the microscope system (e.g. alignment, calibrations, measurements, software updates etc.) that is easily accessible by all users. A good 'rig log' pays dividends in years to come.
  ▲ **CRITICAL** For spatial resolution measurements there must be a motorised vertical translation stage with ≤ 0.5 µm minimum incremental movement
- Pulsed laser suitable for multiphoton excitation with power modulation device built-in or separately installed after the laser
- Objective lens(es) suitable for multiphoton microscopy
- Lens cleaning tissues

- Deionised water%
- Mechanical pipettes and tips (1 to 1000 µL)

PROCEDURE 1: LASER POWER AT THE SAMPLE

- Laser power meter (e.g. Thorlabs PM1000D)
- Power sensor head for laser power meter (varies depending on application, see below)
  ▲ **CRITICAL** Time-averaged laser power is measured with either a photodiode or thermal power sensor. Photodiodes convert light directly into an electrical signal, whereas thermal power sensors convert the thermal energy deposited by the light into a measurable voltage. Thermal power sensors are often recommended because photodiode sensors can saturate depending on the peak powers of your laser, though thermal sensors are slower to respond to power changes, and more sensitive to external conditions. The wavelength range, power range, sensor area and sensor resolution should all be considered when choosing a power sensor: The wavelength and power range should match the lab's imaging needs; the sensor area should be larger than the exit area of your objective to allow sufficient light to get to the active sensor area; and the sensor resolution must be fine enough to give you the accuracy you need.
- Clamping hardware (bolts and clamps) or adhesive (tape, sticky tack) for securing the power sensor to the microscope stage

PROCEDURE 2: FIELD OF VIEW SIZE

- Ethanol
- Gridded microscope slide (Thorlabs part number R1L3S1P or Edmund Optics part number 57-877)
- Autofluorescent plastic slide (Chroma part number 92001)
- Mechanical clamp, adhesive or epoxy resin
- Glass microscope slide
- Nail varnish
- Coverglass
- Copper grid used for electron microscopy (e.g. SPI supplies, part number 2145C-XA). These grids have a pitch of 25 microns with 19-micron wide square holes. Dry copper EM grids will emit light when stimulated by a multiphoton laser.

PROCEDURE 3: FIELD OF VIEW HOMOGENEITY

- Autofluorescent plastic slide (Chroma part number 92001)
- Fluorescein
- Petri dish
- Delicate single-ply wipes (e.g. Kimwipes)
- Epoxy resin

PROCEDURE 4: SPATIAL RESOLUTION

- Bench-top microcentrifuge
- Heated plate
- Microscope slide
- Coverglass of known thickness
  ▲ **CRITICAL** Keep the thickness constant between repeated measurements. Further discussion can be found in Box 4.
- 1.5 mL microcentrifuge tubes
- Low melting point agarose (e.g., #16520050 Invitrogen)
  ▲ **CRITICAL** Low melting point agarose is recommended for the ease of sample preparation.
- 0.2 µm beads (e.g., F8811 Invitrogen)

▲ **CRITICAL** Choose beads with excitation peaks that match the laser wavelengths routinely used for experiments

- Glass slide with a concavity, or well, in the centre (e.g., #632200 Carolina)

PROCEDURE 5: GROUP DELAY DISPERSION OPTIMISATION

- Pollen grain slide (Mixed pollen grain slide, Carolina Biological Supply Company)
- Fluorescein
- Autofluorescent plastic slide (Chroma part number 92001)

PROCEDURE 6: PHOTOMULTIPLIER TUBE PERFORMANCE

- Tritium/phosphor vial 3 x 11 mm (EDCGEAR e.g. https://edcgear.co.uk/products/tritium-vial-1-5mm-x-6mm-capsule, or mixglo.com e.g. https://www.mixglo.com/store/c2/Vials.html)
- SM1 lens tube, 0.5 inch (Thorlabs SM1L05)
- SM1 end cap (Thorlabs SM1CP2M)
- Epoxy resin
- Mounted Pinhole, 500 µm (Thorlabs P500K)
- ▲ **OPTIONAL** Neutral density (ND) filter (e.g. Thorlabs NE10B-A)
- ▲ **OPTIONAL** Narrow bandpass filter (varies depending on configuration)

PROCEDURE

PROCEDURE 1: MEASURING LASER POWER AT THE SAMPLE • TIMING 0.5-2 h

BOX 1: TIME-AVERAGED LASER POWER MEASUREMENT CONSIDERATIONS

This procedure describes the measurement of time-averaged laser power at the sample, i.e. after the objective lens. However, the average power is not the complete picture. Lasers used in multiphoton microscopy are pulsed, which enable vastly improved efficiency for multiphoton excitation[21,71]. The power during a pulse is known as the peak power, which is often orders of magnitude higher than the average power. The peak power can be easily estimated from the average power under the simplifying approximation that the pulse envelope (the "shape" of the intensity profile of the laser pulse) is rectangular:

$$Peak\ power\ (W) = \frac{Average\ power\ (W)}{Pulse\ duration\ (s) \times Pulse\ repetition\ rate\ (Hz)} \quad \text{(eq. 2)}$$

You should consider the peak power and pulse energy as well as average powers when comparing experiments on different microscopes and lasers. Two systems with the same average power could have vastly different peak powers, leading to different amounts of photo-bleaching, emitted fluorescence and photo-damage. Similarly, with changes in laser repetition rate, the pulse energy can be very different for the same average power. The use of lower repetition rate lasers with high pulse energies is common for photostimulation, and for three-photon imaging, where high peak powers are also often required.

The aim of this procedure is to equip anybody with a simple metric for monitoring the laser power reaching the sample on their multiphoton microscope, the time-averaged power. This protocol cannot be used to measure actual peak power, since this requires knowledge of the pulse duration (see **Procedure 5**), and pulse envelope, which is a much more complicated measure.

The way power readings will be taken will depend on your hardware and software. There are three possibilities:

- **Manual readings**: the user must set the power level in software and record the laser power value reported by the power meter console. We have chosen to describe this method.
- **Software calibration**: a calibration process provided by the microscope acquisition software. Note: the calibrated power in microscope software may not be accurate for low values. If you need low values, such as 5 mW, then you should check the correct percent power manually. Calibration curves are wavelength-specific because laser max power and Pockels cell bias voltage both vary with wavelength.
- **Custom software**: a custom software tool that reads values from the power meter console whilst controlling laser power, i.e. a Python script.

! CAUTION Ensure that local laser safety rules are always followed to prevent fire and eye/skin damage. Consult a laser safety officer for advice.

▲ CRITICAL Some steps have multiple possible methods for achieving the result, ensure to maintain consistency when measuring the beam in future iterations of the procedure by recording your decision at each step.

1. Turn on the microscope hardware and software necessary for controlling laser beam scanning and laser shutters.
2. Turn on the laser, and if necessary, select the wavelength normally used for imaging applications.
3. **▲ OPTIONAL** Some laser power modulators, such as Pockels cells, are temperature sensitive. If using such a modulator, open the required shutters so that the beam passes through the device to warm it to an equilibrium temperature. In an ideal setup, there will be a hard shutter downstream of the laser power modulator, and this shutter is used to prevent light from entering the microscope when the beam is “off”.
4. Wait for the laser power output to stabilise. The time taken for stabilisation depends on the laser and can be measured and used in future iterations of this procedure. For the first time, wait at least an hour.
   ? TROUBLESHOOTING
5. **▲ OPTIONAL** If using a Pockels cell, ensure the bias voltage is set to the value when it was last aligned, and keep a log of that number somewhere.
6. Install an objective lens that you want to measure the laser power for into the microscope.
   ▲ CRITICAL STEP Ensure the objective is clean by looking through the bottom of the objective in the room light to magnify the front lens. If it is not, clean the objective lens using a suitable method depending on the type of objective and the contamination. Consult manufacturers recommendations if unsure of the procedure.
7. Plug the power meter sensor connector firmly into the console.
8. Turn on the power meter.
   ▲ CRITICAL STEP Ensure the battery is charged, or it is plugged into a power source to last for the duration of the measurements.
9. Set the power meter console measurement wavelength to match the laser wavelength being measured.
10. Place the sensor under the objective and secure the sensor in place using a suitable method for your stage configuration (bolt/clamp or adhesive).
    ▲ CRITICAL STEP Centre the objective over the active area of the sensor laterally and set the height of the objective such that the laser will not be focused on the power meter’s sensitive surface. It is a balancing act to set the objective-sensor distance. The sensor should be close to, but not at, the objective’s working distance, as this will ensure the sensor captures all light whilst also minimising the chance of damaging it with a tightly focused beam (**Fig. 3b**). More consistent readings will be obtained if the beam fills a large proportion of the sensor, but if light falls outside of the active area an inaccurate result will be obtained.

11. ▲ **OPTIONAL** Apply appropriate immersion media for the objective if the power sensor is designed for it.
12. "Point" or "centre" the beam in the software, so it is stationary in the centre of the field of view. If this is not possible, a similar result is achieved by zooming in by a factor of 10x or 20x and scanning a small area with beam blanking disabled (**Fig. 3a**).
13. "Zero" the power meter to set the reading to 0 mW and remove any background offset.
14. Open any remaining shutters so that the beam passes through the system to the sensor.
15. Find the minimum power by adjusting the software's power modulation control until a minimum reading is seen on the power meter.
16. Record the power meter measurement (usually in units of mW) and the power modulation value in the software (i.e. %, volts, arbitrary units) for this minimum power.
    ? TROUBLESHOOTING
17. Find the maximum power by adjusting power modulation until a maximum reading is reached.
    ! CAUTION Do not exceed the power sensor's upper power limit, otherwise the power sensor surface could become damaged and result in inaccurate readings.
18. Record the power meter measurement and modulation value for this maximum power.
19. Record intermediate laser powers and modulation values that are commonly used in your experiments.
    ▲ **CRITICAL STEP** It is common for modulators to respond non-linearly to the control input so laser power can be a sigmoidal function of the percentage power value, where the maximum power may occur well before "100%" laser power (**Fig. 3c**).
20. Arrange the above power meter measurements and software modulation values in a table of a suitable spreadsheet program for future comparisons.
    ▲ **CRITICAL STEP** Provide information regarding how the reading was made (stationary or scanning beam) and if scanning, report the temporal fill fraction. If you have access to different power meters, report the model number or serial number of the sensor head.
21. Repeat steps 9-20 for any other wavelengths that are important for imaging experiments.
22. Compare new measurements to historical power measurements and ensure that the laser power is not changing.
    ? TROUBLESHOOTING

PROCEDURE 2: MEASURING FIELD OF VIEW SIZE ●TIMING 2 h

BOX 2: FIELD OF VIEW SIZE CONSIDERATIONS

The maximum FOV of an imaging system is defined by the maximum scan angles in the X and Y dimensions and the excitation optics, but the working FOV used in experiments should be driven by the needs of the experiments, and are often based on other characteristics, such as required sampling density, field homogeneity (see **Procedure 3**), field curvature, and distortion. The FOV size is also used in mosaic imaging where tiles of images are acquired in a grid and merged. FOV size is not expected to change from year-to-year, so monitoring its size is not required unless the optics or scanners in the excitation path of the microscope have been changed. Here, we describe how to measure the maximum effective FOV of a laser scanning multiphoton microscope.

We will measure physical dimensions of the imaged FOV at the minimum zoom factor (the largest possible scan angle) and evaluate field distortion based on that image. For this, we will acquire an image of a fluorescent sample with features of known geometrical dimensions and convert this to microns in the X and Y axes.

BOX 3: FIELD OF VIEW SIZE CALIBRATION SAMPLE

The sample can be a microscopy grid overlaid over a Chroma fluorescent slide, or a copper grid used in electron microscopy. Copper grids are cheap, will emit light when stimulated with a multi-photon laser and are robust to damage. They can also be overlaid on top of a Chroma slide to create a negative image.

We note that there are commercial slides available, such as the Axiom Optics Argolight slides that also can be used for such measurements. These types of slides have been used with good success for microscopes employing single photon excitation. They are significantly more expensive than the options we provide here, and can be damaged by very intense laser pulses, so should be used with care.

1. Turn on the microscope hardware and software necessary for controlling laser beam scanning.
2. Turn on the laser and wait for the power to stabilise (see **Procedure 1**). Select the wavelength normally used for imaging applications.
3. Prepare the relevant calibration sample (see **Box 3** for considerations) for field of view size measurements according to the equipment you have:
   A. ▲ **OPTIONAL** Prepare a gridded slide.
      i. Clean a gridded microscope slide and an autofluorescent plastic slide using single-ply wipes and ethanol.
      ii. Place the autofluorescent plastic slide flat on a bench.
      iii. Identify which side of the gridded slide has etchings.
      iv. Add a droplet of water onto the autofluorescent plastic slide and place the gridded slide such that the etchings face the autofluorescent slide.
      v. Clamp the two slides together with a mechanical clamp, adhesive or epoxy resin.
   B. ▲ **OPTIONAL** Prepare a copper grid.
      i. While keeping the grid dry, place it on a conventional glass slide or an autofluorescent slide (for a bright negative image of the grid).
      ii. Place a coverslip over the top of the grid.
      iii. Seal the coverslip with nail varnish.
4. Install an objective lens in the microscope that you routinely use for imaging.
5. Place the sample under the objective lens.
   ▲ **CRITICAL STEP** Place the sample perpendicular to the optical axis to eliminate any tilt with respect to the imaging plane.
   ▲ **OPTIONAL** It is possible to use the microscope's laser beam to align the sample to the objective and reduce tilt. For this, lower the laser power such that no more than a few mW exits the objective. Close any iris in the excitation path to only let through the very centre of the beam. Make sure the beam hits the sample and then use an infrared (IR) viewing card and an IR viewer to visualise the reflected beam. Here, the reflection will be very weak, on the order of 1-5%, so an IR viewer is needed to visualise it. Adjust the sample tilt such that the reflected beam propagates directly along the incident beam.
6. Apply any immersion media appropriate for the objective lens and position the lens at roughly its focal distance away from the sample.
7. Focus on the calibration sample gridded surface.
   ▲ **OPTIONAL** If using a fluorescent slide overlaid with a grid, image the very surface of the fluorescent slide to get a negative image just underneath the grid (**Fig. 4b**).
8. Acquire an image of the calibration sample at the minimum zoom to give the largest FOV (**Fig. 4a, 5a**).
   ▲ **OPTIONAL** If the system has field curvature or a large FOV (>1 mm), it might be difficult to obtain a completely flat image of the sample. In this case, it is necessary to acquire a z-stack that covers the axial extent of the tilted imaging plane and make a maximum projection of that stack for the next steps.
9. Record the number of whole grid squares required to cover the width and height of the FOV.

▲ **CRITICAL STEP** If the sample is rotated so the grids don't run horizontally or vertically, rotate the sample to match the grid rows/columns with the X and Y axis of the image.

▲ **OPTIONAL** As counting the lines of a copper EM grid is time consuming, using an automated tool may be preferable (Grid2MicsPerPixel tool[72], **Fig. 4c**).

10. Record the total number of pixels required to cover the same distance in step 9.
11. Multiply the number of grids from Step 9 by the grid pitch size in microns to give the total width and height in microns.
12. Divide the distance in pixels from Step 10 by the distance in microns from Step 11 to get the micron-to-pixel conversion and multiply that by the total pixels in the image to get the FOV size.
13. Evaluate whether there is pincushion or barrel distortion[73] in the images (**Fig. 4b**). Presence of these aberrations would signify an off-axis optical performance degradation in the system.

? TROUBLESHOOTING

14. Repeat steps 4-12 for any other objectives used for imaging, as calibration is only relevant for the objective used to do that calibration.

▲ **CRITICAL STEP** Calibration files are usually saved for each objective in the acquisition software so that the pixel size is calibrated for every acquired image without any manual metadata editing.

15. ▲ **OPTIONAL** If the microscope has other imaging paths, repeat the measurement for one objective using these imaging modalities (e.g. epifluorescence or brightfield, **Fig. 5a, b**) and note any rotation/mirror effects between the two imaging modes, which will be the same for all objectives.

PROCEDURE 3: ASSESSING FIELD OF VIEW HOMOGENEITY ●TIMING 2 h

▲ **CRITICAL** This procedure describes how to assess the homogeneity of the field of view by imaging a uniform fluorescent sample and measuring how the image intensity varies across the image. The resulting measurements are a description of the overall system's performance, meaning that any drop-offs in intensity could be caused by optical degradation in either (or both) the excitation and collection paths.

1. Turn on the microscope hardware and software necessary for controlling laser beam scanning.
2. Turn on the laser and wait for the power to stabilise (see **Procedure 1**). Select the wavelength normally used for imaging applications.
3. Install an objective lens in the microscope that you routinely use for imaging.
4. Prepare a thick uniform fluorescent sample, either an autofluorescent plastic slide (cleaned with ethanol and single-ply wipes) or a fluorescein bath (if using a water-dipping objective) with 1 µL of fluorescein to 10 mL of water inside a suitable petri dish.

   ▲ **CRITICAL STEP** Many objectives used for *in vivo* multiphoton imaging have field curvature, where the imaging plane is not actually a plane, but is instead shaped like a shallow bowl (see **Procedure 2** to measure this). This is particularly noticeable for some large FOV systems[42,74,75]. To eliminate the effect of small field curvature on field homogeneity, the sample for this measurement should be sufficiently thick that the beam remains in the sample across the entire field.
5. Place the sample under the objective lens and focus on it (dip water immersion lenses directly in the fluorescein).
6. Set the laser power to <5 mW (see **Procedure 1** to measure this).
7. Begin imaging and turn the PMT gain up from 0 until signal from the sample is seen.

   ▲ **CRITICAL STEP** The PMT gain should be turned up slowly to avoid damaging the PMTs with a potentially very bright sample. If no signal is seen, adjust the objective focus up and down to search for signal from the sample before turning up the PMT gain further.

8. ▲ **OPTIONAL** If using a fluorescent slide, find the sample surface then slowly lower the objective until all hints of the surface inhomogeneities have vanished. You will probably need to focus about 100 to 200 microns deep.
9. Acquire an image of the sample using the largest FOV size the system allows for.
   ▲ **CRITICAL STEP** The width/height of the image in pixels needs to be sufficient to sample the inhomogeneity. Additionally, an average of multiple images is advisable to reduce noise.
10. ▲ **OPTIONAL** If this is the first time you are performing the measurements, acquire more images using higher zooms (smaller FOVs) at 50% and 25% of the full FOV, for example. This will help diagnose uncommon inhomogeneities that could arise from the laser power modulator.
    ? TROUBLESHOOTING
11. ▲ **OPTIONAL** If the saved image is not already scaled correctly, translate pixels to microns using the FOV size calculated in **Procedure 2**.
12. Normalise the image by dividing all pixel values in the image by the maximum pixel value.
13. Plot a line profile through the horizontal/vertical axes and through the diagonals of the FOV (**Fig. 6a**). The horizontal/vertical profile is informative about each scan axis (from the X or Y scanner; **fig 6b**).
14. Evaluate how symmetrical the brightness across the FOV is. Because of the radial symmetry of most optical systems, a well aligned microscope should have the brightest part of the field in the centre of the image and the brightness should fall off evenly around the centre.
    ? TROUBLESHOOTING
15. If previous measurements have been made, refer to them to determine if there have been any changes in homogeneity that need addressing.
    ? TROUBLESHOOTING

PROCEDURE 4: MEASURING SPATIAL RESOLUTION ●TIMING 3.5 h

BOX 4: SPATIAL RESOLUTION CONSIDERATIONS

A standard method to measure the excitation volume shape is to image fluorescent beads that are small enough to approximate an “impulse” function. That is, fluorescent beads that are smaller than the expected excitation volume. Beads with a diameter of 0.2 µm are commonly available and are smaller than most multiphoton systems’ excitation volume when near-infrared (>700 nm) light is used. These are sometimes called “sub-resolution” beads. The beads can be spread across a microscope slide or embedded in a 3D tissue phantom[76] (e.g. agarose). Of course, even these small beads are not true impulse functions, but in practice they are a close enough approximation that the resulting measurements are useful for characterising a system. Imaging small structures *in vivo* can provide a rough proxy for bead measurements. However, biological features are not proper impulse functions either and they are typically extended in some dimension. Moreover, a non-zero background signal can distort excitation volume measurements from small structures. Therefore, measurement using sub-resolution fluorescent beads on a slide provides a better baseline for comparisons over different time points and different imaging systems.

Coverglass thickness is an important variable in measuring spatial resolution due to spherical or chromatic aberration increasing with coverglass thickness. This is especially true with higher numerical aperture objective lenses and those designed for air or water immersion, for example. The coverglass thickness should remain the same for comparisons over different time points and different imaging systems.

▲ **CRITICAL** As the resolution is a function of wavelength, the measurements should be performed with excitation/emission wavelengths close to those used in experiments (**Fig. 7**). Lens designs, anti-reflective coatings, dichroic filters, and mirrors all have wavelength-dependent properties and can

influence the measurements made.

1. Turn on the microscope hardware and software necessary for controlling laser beam scanning.
2. Turn on the laser and wait for the power to stabilise (see **Procedure 1**). Select the wavelength normally used for imaging applications.
3. Prepare the bead slide:
   a) Make a 0.75% (wt/vol) agarose solution by dissolving 0.150 g low melting point agarose in 20 mL water at ~75° C.
   b) Vortex the agarose solution until completely dissolved.
   c) Add 1000 µL of the agarose solution to a 1.5 mL microcentrifuge tube and wait for the agarose to cool slightly to 50°C.
   d) Add 4 µL of 0.2 µm beads (e.g., F8811 Invitrogen) to the 0.75% (wt/vol) agarose solution to reach a dilution of ~1:5000 in volume.
   e) Vortex the mixture for 5 seconds and then spin it down for 5 seconds with a bench-top centrifuge to make the mixture uniform and remove bubbles.
   f) Transfer the bead/agarose mixture in to the concavity of a welled glass slide, and cover with a coverglass of known thickness (e.g., #1, #1.5, ...).
      ▲ **CRITICAL STEP** Avoid bubble formation during the process and completely fill the space between the slide and the cover glwipeass with the mixture, leaving no air gap. Air gaps and bubbles can move around during the imaging session and cause movement of the beads.
   g) Wait for 15 minutes for the mixture to completely cool down and solidify.
      ▲ **CRITICAL STEP** (Optional) If planning to keep the slides for longer than 2 hours, seal the sides of the coverglass (e.g. nail polish, wax, optical glue etc.) to prevent evaporation.
4. Install an objective lens that you routinely use for imaging in the microscope.
5. Place the prepared slide under the objective lens on a motorised stage and use the imaging system to find the focal plane of the beads with a FOV size of 100-200 µm.
   ▲ **CRITICAL STEP** The laser power should be close to the minimum required to clearly identify individual fluorescent beads. If higher powers are used, there is a risk of over- or underestimating the excitation volume, through either saturation or bleaching respectively, and this issue is exacerbated when using fluorescence molecules with relatively large cross sections[21].
   ? TROUBLESHOOTING
6. Zoom-in to a pixel size of ~0.04 µm and plot the intensity of multiple putative single beads and small clusters of beads as a histogram. This process will reveal a series of peaks where each peak will be a multiple of the intensity of a single bead. If sufficiently sampled, the interval between peaks will be regular and equal to the intensity of a single bead. Use this information to verify if a region of interest is a single bead.
7. Identify a single, isolated bead with a non-saturating intensity.
   ▲ **CRITICAL STEP** Ensure there are not any other beads in the axial scan range of the chosen bead, as this would interfere with the measurement.
   ▲ **CRITICAL STEP** Additionally, the field-of-view should be large enough to ensure that the bead intensity returns to background levels, but no other beads should be present in that space.
   ▲ **CRITICAL STEP** Examine the bead intensity and ensure the pixel intensity at any image plane does not saturate the PMT (i.e. very few pixels reach the maximum possible intensity value e.g. 65,536 for a 16-bit image). If that occurs, lower the laser power or the gain of the PMT, or find another suitable bead.
   ? TROUBLESHOOTING
8. Acquire a z-stack of the bead with a 0.3 µm step size and appropriate total axial range.
   ▲ **CRITICAL STEP** Select the total range of the stack to be 4-6 times larger than the theoretical axial extent of the PSF. For example, for a system with an axial FWHM of 5 µm in theory, use 20-30 µm z-extent.
   ▲ **CRITICAL STEP** The lateral pixel size and axial stage movement should be calibrated correctly using a structured sample (see **Procedure 2** for lateral pixel size), rather than using the stage motor values.

9. Fit the intensity measurement with Gaussian curves in the lateral (XY) and axial (Z) direction, respectively (**Fig. 8**). We provide a tool[72] for conducting such analyses in MATLAB. Another option is Python-based[77] and can easily extract PSFs from multiple beads in a single image.
   ▲ **CRITICAL STEP** In cases where the excitation volume is very tilted in Z, the Gaussian fit procedure should account for this tilt, otherwise the excitation volume will be underestimated. The current version of our example code does not include a subroutine to correct the tilt. One could use a built-in rotation function, such as ImageJ ('Image->Transform->Rotate…') and MATLAB ('imrotate'), to correct the tilt.
   ? TROUBLESHOOTING
10. Find the full width at half maximum of the curves in units of length (e.g., nm or µm) and use these values to keep track of the resolution.
    ▲ **CRITICAL STEP** When referring to a theoretical or expected resolution, be sure to include the equation, the values for any parameters in the equation, and a paper reference, e.g. Zipfel et al. 2003[21]. Be clear whether FWHM, 1/e radius, or $1/e^2$ radius of the PSF is reported. This provides clarity to the reader and enables fair comparisons.
11. Repeat steps 7-10 for three or more beads to achieve confidence in the resolution measurement.
12. Repeat steps 7-11 for multiple locations in the field-of-view: the centre, the edges of the X scan, the edges of the Y scan, and different depths. It is useful to show where resolution breaks down. Instead of simply reporting the best values, show where the resolution starts to degrade and by how much. For routine checks, measuring at just two or three reference locations can be sufficient.
    ▲ **CRITICAL STEP** It is recommended that beads are measured at different locations across the field-of-view (centre and towards the edges) and at different depths. Optical aberrations tend to increase away from the centre of the field-of-view, while spherical aberration and scattering vary over the imaging depth.
    ▲ **CRITICAL STEP** Zoom-in on beads at the edge of the field-of-view by offsetting the scan centre of the linear galvanometer scanner. This offsetting function might appear as 'shift', 'offset', or 'park' on the microscope control software.
    ▲ **CRITICAL STEP** If an air immersion objective is used, due to the difference between the refractive index of the objective immersion medium (e.g., air) and the specimen medium (e.g., water), the actual focal position (Δfocus) within the specimen is moved a different amount from the stage movement (Δstage). Therefore, a correction factor is required to convert the axial stage movement to the actual focal movement. According to the reference[34], a simplified calculation of the correction factor is,

$$\frac{\Delta\, focus}{\Delta\, stage} = \frac{tan(sin^{-1}\frac{NA}{2n_1})}{tan(sin^{-1}\frac{NA}{2n_2})} = \frac{n_2 cos(sin^{-1}\frac{NA}{2n_2})}{n_1 cos(sin^{-1}\frac{NA}{2n_1})} = \sqrt{\frac{4{n_2}^2 - NA^2}{4{n_1}^2 - NA^2}} \qquad \text{(eq. 3)}$$

    where n_1 is the refractive index of the immersion medium, n_2 is the refractive index of the sample, and NA stands for numerical aperture of the objective.

PROCEDURE 5: OPTIMISING GROUP DELAY DISPERSION ●TIMING 1.5 h

BOX 5: GROUP DELAY DISPERSION CONSIDERATIONS

The art and practice of dispersion control is rich, and strongly dependent on the equipment at hand[78–80]. Beyond that, there is a plethora of instantiations for building external compensation modules, or general dispersion control, the details of each is beyond the scope of this protocol, especially if higher order dispersion control is necessary.

This procedure will assume that the user has a form of an easily tuneable dispersion control module, and will use the level of fluorescence generated following two-photon excitation as a surrogate for measuring changes in the pulse width. The goal is to collect image intensity data throughout the range of GDD correction values, and ideally, find the dispersion compensation setting that corresponds to the brightest image. This would correspond to the shortest laser pulse that your system can deliver, and hence the highest peak intensity of the laser, for a given average laser power. The fluorescence can be used because the signal is proportional

to the laser intensity squared, while the intensity is proportional to the average power/pulse width, as described earlier. If the lab has invested in an autocorrelator, using that will provide a more quantitative assessment of the pulse width, though the method described above is a reasonable alternative for fast optimization.

If you do not have either dispersion control nor an autocorrelator, how concerned should you be about laser pulse management? Dispersion management/compensation becomes less important for simpler optical paths and longer initial pulses (due to pulse broadening being nonlinearly proportional to the pulse width). If you have a relatively simple microscope, with few optical elements (e.g. mirrors, galvanometer-based mirror scanners, scan lens, tube lens, objective) between your laser and the sample, and your laser has initial pulses of ~150 fs, dispersion compensation may not be a worthwhile investment. If neither of these conditions hold, it may be worthwhile to consider working with either another lab or a vendor to measure the laser pulse on sample with an autocorrelator to see if additional measures are needed. This is especially important for short pulse laser systems. For example, for a system with a total GDD of 6000 fs^2, a 60 fs pulsed laser will be broadened to 284 fs, an almost 5x increase, and concomitant 5x decrease in total fluorescent generated, while a 150 fs laser pulse will be broadened to 186 fs, only a 1.24x increase in pulse duration and 1.24x less total fluorescence. We note that for intensity levels below saturation, though the instantaneous two photon efficiency drops by the square of the pulse duration increase, the total generated fluorescence loss scales linearly with pulse width through equation 4, as the relative duty cycle increases with increasing pulse duration.

1. Turn on the laser and wait for the power to stabilise (see **Procedure 1**). Select the wavelength normally used for imaging applications.
2. Turn on the microscope hardware and software necessary for controlling laser beam scanning.
3. Install a microscope objective lens used for imaging experiments.
4. Prepare the sample and place it under the objective lens:
   a) For water immersion dipping objectives, fill a petri dish with a fluorescein bath of 1 µL fluorescein in 10 mL water
   b) A fluorescein drop under a coverslip, dilute 1 µL fluorescein in 10 mL water and 50 µL drop under the coverslip
   c) Autofluorescent plastic slide
   d) Pollen grain slide
5. Apply any immersion media appropriate for the objective lens and position the lens at roughly its focal distance away from the sample
6. Begin live scanning and focus on the sample.
   ▲ **CRITICAL STEP** If using a slide with features (e.g. pollen grains), use a higher magnification so that the smallest feature chosen occupies ~50 x 50 pixels. If sized like this, it ensures that any small motion or pixel alignment errors will not significantly corrupt the measurements. However, if magnification or laser power are too high, bleaching and damage to the pollen grain may occur.
7. Open a live histogram of pixel intensity values from the image.
8. Set the vertical scale (number of pixels) to “logarithmic” to see the low pixel counts such as those between 1 and 100.
9. Set the x-axis to show the full range of possible pixel values and adjust laser power and/or PMT settings so that live pixel values occupy 25% of the full range. Once these laser power and PMT settings are set, these cannot change for the duration of the measurements. If they change, the steps below will need to be repeated.
   ▲ **CRITICAL STEP** High laser powers result in more photobleaching, which interferes with the interpretation of the measurement. The preference would be to first turn down the laser power, rather than the PMT voltage.
10. Adjust the pixel intensity range on the histogram to show 50% of the full range (**Fig. 9**), and record/remember the maximum pixel value. If the histogram display also shows the mean and max values of the image, record that too.
11. Continue imaging for at least 2 minutes and compare the current pixel values with the values noted in step 10. If the values are significantly different, it shows that either the sample is bleaching and/or the system is not stable. Find either a more stable sample, or turn the laser power down to decrease photobleaching, such that the pixel histogram is stable for ~2 min.

▲ **CRITICAL STEP** The signal needs to be stable to continue this protocol because the absolute pixel values need to be compared across time as the dispersion compensation is adjusted.

12. Record the current dispersion compensation setting of the laser (usually in fs^2 GDD) or external module and record the shape of the histogram alongside the mean and max pixel values.
13. Change the dispersion compensation by a fixed amount (increments of ~2000 fs^2 GDD are generally sufficient).
14. Examine the live histogram and again record the shape of the histogram alongside the mean and max pixel values.
15. Continue repeating steps 13 and 14 in the positive direction from the initial setting, and then repeat in the negative direction. If the mean pixel value drops >30% from the initial recorded value, do not continue in that direction.
    ? TROUBLESHOOTING
16. Plot the mean pixel values of the image as a function of dispersion compensation values (**Fig. 10**). Identify the GDD value that gives the highest mean pixel value.
17. Now repeat steps 12 to 15 around the GDD value in step 16 to find the exact best GDD compensation, this time with increments of ~250 fs^2 GDD. The dispersion compensation setting that gives the highest mean pixel value is the one you want to use for your experiments.
18. Repeat steps 6 to 17 for the different wavelengths and objectives that will be used for imaging.
    ? TROUBLESHOOTING

PROCEDURE 6: MEASURING PHOTOMULITIPLIER TUBE PERFORMANCE ●TIMING 3.5 h

BOX 6: CONSIDERATIONS FOR MEASURING PHOTOMULTIPLIER TUBE PERFORMANCE

In this procedure, we describe a simple protocol to quantify light detection performance. With minor variations, the procedure can be used to test either the entire collection system (defined here as objective, collection optics and PMT), or test a PMT directly. Direct tests of the PMT require it to be disconnected from the microscope, but otherwise require minimal modification to the procedure. We note that this procedure does not provide measurements in physical units, nor does it test different aspects of PMT performance as might be reported on the datasheet (e.g. anode luminous sensitivity), which requires additional sophisticated instrumentation and is beyond the means of most research labs. Instead, we present a procedure that provides a robust, relative measure of performance that can be used comparatively, e.g. to compare several PMT units of the same model or monitor performance of the same unit over time.

The measure is based on ideas from signal detection theory and is not specific to PMTs – indeed, the protocol can be applied to any light detector (e.g. hybrid detectors). Finally, it also allows the user to select the optimal operating point (typically referred to as “gain”) for a specific PMT unit. The gain of a PMT is adjusted by changing the high voltage (HV, typically 500 to 1500 V) that is distributed across its electrodes. In most instances, the user will control HV via a lower voltage control signal (e.g. 0 to 5 V) that is provided to the socket assembly or PMT module. Users should be aware of how gain is controlled on their specific system. We recommend performing this procedure at least once every 6 months for routine monitoring of PMT performance.

This protocol requires a light source with a stable output. Such sources are available commercially, e.g. based on closed-loop control of an LED, or can easily be assembled using a tritium vial as an approximately constant light emitter[81], as we have chosen to do for this procedure. Tritium is a radioactive isotope of hydrogen with a half-life of 12.3 years. Tritium vials contain a small amount of tritium gas and a phosphor coating that produces light by radioluminescence when bombarded with beta particles. Vials are widely available with phosphor coatings that produce various colours including ‘red’ and ‘green’. These work well over the duration of most experiments, although additional care must be taken when analysing

measurements made across years; first, the half-life of tritium will cause a well-defined decrease in intensity, and secondly, phosphor degradation will further impact long term stability[82].

To evaluate the performance of a detector, we need to consider not only the measurements made with the light source but also the background response obtained under dark conditions. Dark currents increase with gain, vary between PMT units, and can change over the lifetime of the PMT.

Although pixel grayscale values and SNR are informative, we recommend using ROC-AUC analysis as the best means to compare PMT units and track performance over time. Based on ideas from signal detection theory, ROC-AUC analysis enables comparison of the pixel value distributions obtained with the light source versus under dark conditions: A good detector will produce separated distributions with minimal overlap, which will be reflected by a large ROC-AUC value. SNR partially addresses this but does not consider the distribution of pixel values in light response images, which is a product of several factors including shot noise, multiplication noise and gain.

We will illustrate the data analysis and interpretation using:

- Measurement data from several units of the same multialkali PMT model (Hamamatsu R10699) when first installed ("day one" performance)
- Measurement data from a single R10699 when first installed and then after a long period of routine use
- Measurement data from two GaAsP PMT units (Hamamatsu H10770PB-40)

1. Prepare the tritium/phosphor light source:
   a) Select a tritium vial of the appropriate colour for the detection channel being tested (e.g. 'red' or 'green') or use a 'white' tritium vial for testing multiple colour channels.
   b) Use a small drop of epoxy resin to affix the tritium vial to the centre of the inside surface of the SM1 end cap and allow the resin to set overnight (**Fig. 11**).
   c) Screw the end cap, with the mounted tritium vial, onto the lens tube.
   d) **▲ OPTIONAL** Add a neutral density filter to reduce light intensity, and/or a diffuser to reduce inhomogeneity, if required.
   e) **▲ OPTIONAL** Add a narrow bandpass filter to limit the spectral bandwidth of the light source. This is recommended if the light source will be used to compare the collection system of different microscopes.
   f) At the open end of the lens tube, attach a mounted pinhole (**Fig. 11**).
   g) Label the assembled tritium source with a unique reference number, assembly date and 'colour' of the tritium vial (e.g. 'red').
   h) Once assembled, the tritium source can be used for many years. To ensure stability, it must not be assembled/disassembled and should be stored in a dust-free container.
2. Install the PMT in the microscope to test the entire collection system and install a microscope objective lens used for imaging experiments. Keep this objective lens consistent for all future readings.
3. **▲ OPTIONAL** Install the PMT in custom optomechanics at a fixed distance from the light source to test the PMT independently from the remainder of the collection system.
4. Turn on the microscope hardware and software necessary for controlling image acquisition.
   ▲ CRITICAL STEP Refer to previous measurement metadata to ensure consistency of instrument software settings and hardware configuration across tests. Relevant factors include transimpedance amplifier settings, microscope hardware (including emission filters), and image acquisition settings.
   ▲ CRITICAL STEP Take precautions to prevent any stray light from reaching the PMT, by building a light-tight chamber to surround the microscope and switching off room lights. Additionally, switch off or close laser shutters to prevent any laser light from affecting measurements of PMT

performance.

5. Operate the PMT at a normal gain (voltage) while shielding it from any light for around one hour prior to testing to ensure stable operation.
   ▲ **OPTIONAL** For new PMTs, or a PMT that has been unused for several months, it may be desirable to first "age" the tube by operating it for several hours as this can improve stability.
6. Make a record of the room temperature, because PMT performance is dependent on temperature.
   ▲ **CRITICAL STEP** Room temperature should match that at which experiments are routinely conducted and be consistent within and across tests.
7. Measure the response of the detector under dark conditions (the 'dark response') by collecting a short time-series of images (few seconds duration) at each PMT gain setting for a range of gain values. A time-series is taken such that a middle-of-series single image can be used for analysis and avoidance of artefacts on the "start" or "stop" frame. For testing the Hamamatsu R10699 with C6270 socket assembly, a range of control voltages from 0 to 3.5 V in 0.25 V steps was used, which corresponds to 0 to 900 V across the PMT electrodes.
   ▲ **CRITICAL STEP** An image must be acquired at zero gain to determine any image value offsets unrelated to the PMT itself.
   ▲ **CRITICAL STEP** Care should also be taken not to exceed the maximum HV indicated on the datasheet for the specific model of PMT
8. Place the constant light source under the objective lens (if testing the entire collection system) or PMT window (for direct PMT tests).
   ▲ **CRITICAL STEP** If using a tritium light source as described above, place the pinhole directly beneath the objective. Move the objective very close to the pinhole, for example to the lip of the pinhole mounting. Do not use immersion media.
9. Stream live image data and slowly raise the PMT gain to a normal operating level (according to prior imaging experiments).
10. Monitor the grayscale values (mean or histogram) while adjusting the lateral position of the light source using the X/Y motorised stage controls to maximise the intensity of the image, thereby centering the pinhole on the objective lens.
    ▲ **CRITICAL STEP** If this is a new tritium light source, or a new model of PMT, take care to slowly increase the PMT gain. Image brightness (mean pixel grayscale value) should be similar to biological samples typically used in the lab. If the images appear too bright, add a neutral density filter to the light source (see **Box 7**).
11. Collect a set of consecutive time-series images of the 'light response' at the same PMT gain settings used for the dark response tests in step 7.
12. Calculate the 'black point' by computing the mean pixel value in the dark response image acquired at zero gain in step 7.
13. Subtract the black point value from all the images of both the dark response and light response series.
14. Compute the mean and standard deviation across all pixels for each image.
15. Plot the mean pixel value at each gain setting (represented as either control signal voltage or high voltage, HV) for the light response image series.
    ▲ **CRITICAL STEP** It should be observed that the mean pixel value increases as a function of gain, owing to increased PMT amplification. In **Fig. 12**, which compares "day one" performance of three R10699 units, AFN9975 produces the highest pixel values as expected from it having the highest test sheet anode luminous sensitivity.
    ▲ **CRITICAL STEP** **Fig. 13** shows measurement data for a single unit (AHB4783 from **Fig. 12**) when first installed and then after approximately 18 months of routine use in one author's lab. Mean pixel values have declined substantially over this time.
    ▲ **CRITICAL STEP** If using a tritium light source, some decline in mean pixel value should be expected due to the radioactive decay of tritium. This can easily be computed by multiplying by a factor *k*, given by,

$$k = e^{-\frac{d}{\tau}} \qquad \text{(eq. 4)}$$

    where *d* is the interval between measurements (in years) and *tau* is the decay time constant of tritium (17.75). The dashed curve (**Fig. 13a**) was obtained in this fashion and shows that the expected tritium decay would only account for a small fraction of the observed decline.

16. Compute signal-to-noise ratio (SNR) at each gain setting, *g*, as the difference in mean pixel value between the light response and dark response images, divided by the standard deviation of the dark response image:

$$SNR_g = \frac{\mu_{light} - \mu_{dark}}{\sigma_{dark}} \qquad \frac{\mu_{light} - \mu_{dark}}{\sigma_{dark}} \qquad \text{(eq. 5)}$$

For example, **Fig. 12** shows that SNR increases as a function of gain and that unit AFN9975 achieves higher SNR than the other two units. **Fig. 13** shows that SNR declines over time.

17. Perform ROC-AUC analysis at each gain setting, using the distributions of pixel grayscale values in the light response image and corresponding dark response image. **Fig. 14** shows such pixel value distributions with the tritium source (red) and under dark conditions (black) at a variety of gain settings for an example PMT. At each gain setting, ROC-AUC values (indicated at the top of each figure panel) quantify how well separated the two distributions are.
▲ CRITICAL STEP ROC-AUC initially increases with gain before reaching a plateau (**Fig. 14**). Moreover, although unit AFN9975 has the highest anode luminous sensitivity, highest pixel values and highest SNR, it does not have the best performance as measured by ROC-AUC. Rather, unit AFK8564 has marginally better performance as judged by the fact it plateaus at a slightly higher ROC-AUC value. Unit AHB4783 is notably poorer, despite having similar pixel values and SNR versus the best performing unit, which is likely due to its high variance (not shown). **Fig. 13** shows that ROC-AUC values decrease substantially over 1.5 years of routine use. **Fig. 15** shows measurement data from two GaAsP PMT units (Hamamatsu H10770PB-40) installed in a microscope after multiple years of usage.
▲ OPTIONAL The ROC-AUC analysis can also be used to guide the choice of PMT gain settings to use during imaging experiments. Specifically, the choice of gain setting should consider:
a) ROC-AUC performance. Ideally a gain setting will be selected close to the plateau of the ROC-AUC curve.
b) HV across the PMT electrodes must not exceed the maximum value stated on the datasheet and should ideally be 20% below this value. Excessive HV can cause field emission from the dynodes and substantially shorten PMT life[47].
c) Anode current should be kept within safe limits, typically no more than a few µA. Refer to the datasheet for specific PMT models.

Anode currents can be estimated at each gain settingsetting using the mean pixel grayscale value of the light response image along with knowledge of the TIA and ADC settings:

$$I_{anode} = \frac{\mu_{pixel} \times ADC_V}{ADC_{px}} \times TIA_g \qquad \text{(eq. 6)}$$

where, μ_{pixel} is the mean pixel grayscale value of the light response image at a given gain setting; ADC_V is the voltage that the digitiser will map to the highest grayscale value (e.g. 1 V); ADC_{px} is the corresponding grayscale value (e.g. 2048); TIA_g is the gain of the transimpedance amplifier (e.g. $100*10^{-6}$A/V). Consider unit AHB4783 when it was first installed (**Fig. 12**, red curve). ROC-AUC increases with gain but starts to plateau at a control signal voltage of 3250 mV. The corresponding HV is safely below the limit for this PMT model and mean anode current is acceptable at around 5 µA. Thus, this gain setting would be chosen for imaging experiments.

PROCEDURE 7: ESTIMATING ABSOLUTE MAGNITUDES OF FLUORESCENCE SIGNALS

●TIMING 3 h

BOX 8: ESTIMATION OF PHOTON SENSITIVITY

Light, with its stochastic, quantal nature, leads to unavoidable fluctuations in measured signal intensities, commonly termed as "shot noise," "quantum noise," or “Poisson noise.” An optimised microscope will function in a photon noise-limited mode, where other sources of noise have been minimised, leaving only the inevitable quantum noise as significant.

The statistical features of quantum noise follow the Poisson probability distribution, as photon

detections are independent discrete events. However, additional factors like the high-frequency pulsing of laser power, the PMT's inherent gain stochasticity, and noise from the amplification process, add complexities. As a result, photons do not appear as discrete events in the signal and, for a given number of detected photons, the recorded pixel intensity will vary substantially. Additionally, the Analog-to-Digital Converter (ADC) may introduce a bias and additional non–Poissonian electronic noise.

Yet, despite these complexities, the detected noise retains its essential Poissonian trait: the variance of quantum noise is linearly proportional to signal intensity, and the slope of this linearity reveals the *photon sensitivity*, the average increase in measured light per detected photon. Other sources of noise may add on top of quantum noise, but they may be recognized and isolated by their non-Poissonian traits. Finding a linear dependency between signal intensity and its variance provides a strong indication of the quantal nature of the noise. Accurately estimating the photon sensitivity allows effective translation of measured intensities into photon counts.

The following procedure estimates the photon sensitivity directly from the experimental data. For more detailed and deliberate diagnostics and troubleshooting, investigators are encouraged to use a standard static fluorescent preparation featuring a wide range of fluorescence levels, following the same procedure. The photon sensitivity is a stable property of the system since it is controlled by the PMT gain and gains applied by the acquisition system; it is insensitive to many other aspects of the imaging configuration such as magnification, the numerical aperture, laser power, etc. However, the photon transfer curve and the photon counts can describe both the quality of the fluorophore expression and the microscope's imaging performance.

BOX 9: PHOTON TRANSFER CURVE

The principal tool for this estimation is the Photon Transfer Curve (PTC), which plots the variance of detected intensities against intensity values[83]. It is a remarkable fact that the relatively simple calculation of PTC provides so much insight into the properties of the image acquisition process in diverse imaging scenarios. The PTC can be derived from imaging a static fluorescent object over a short time and estimating the noise variance across a wide range of detected intensities.

However, for convenience, we can calculate the PTC during regular experiments in the presence of physiological signals and motion. In this case, the effects of the quantum noise must be isolated from other sources of signal variance. In contrast to quantum noise, dynamic fluorescence fluctuations, such as neuronal activity or tissue movement, produce temporal variances that scale quadratically with intensity. They also have correlated spatial and temporal structures, whereas quantum noise stays decorrelated. The ability to differentiate between the Poissonian quantal noise from other sources of variance enables robust estimation of photon sensitivity even during regular experiments in the presence of physiological signals and motion, without the need for a separate procedure. Estimating the PTC from the experimental data ensures consistency with acquisition settings, contributing to the efficiency of the process. For more deliberate troubleshooting, repeating the procedure with a static fluorescent preparation helps in producing more accurate results.

Figure 16 presents the outcomes of PTC estimation derived directly from experimental data using a 500-frame sequence taken from the MICRONS dataset[84,85] and following the procedure described here. The implementation example can be accessed at the GitHub repository https://github.com/multiphoton-tools/compress-multiphoton. This implementation

includes examples from a variety of projects, accessed through the DANDI Archive.

1. Extract a sequence (X) of approximately 500 frames from a raw imaging sequence before any processing such as motion correction or filtering.
2. ▲ **OPTIONAL** (applicable to systems with resonant scanners) Equalise photon sensitivities by rescaling the image intensity according to estimated laser dwell times at each pixel to restore uniform photon sensitivity across the image. This step reverses the gain compensation performed by the acquisition system and can aid in more accurate photon sensitivity estimations. We did not include this step in our implementation example.
3. ▲ **OPTIONAL** Exclude regions near image boundaries where laser blanking and mirror vibrations might affect measurements. In our example implementation, we excluded 4-pixel margins around image boundaries.
4. Determine the rounded mean values $M = [\frac{1}{2}X' + \frac{1}{2}X]$ and the squared difference values $D = \frac{1}{2}(X' - X)^2$, where X' is X delayed by one frame.
5. Construct count, intensity, and variance vectors**:**
   a) Let vector I represent all unique pixel intensity values in M.
   b) Construct the count vector C so that each element C_j contains the number of pixels k for which $M_k = I_j$.
   c) Compute the variance vector V so that each element V_j contains the average value of D_k across all pixels k for which $M_k = I_j$.

   ▲ **CRITICAL STEP** Calculating means and variances from the differences between adjacent frames offers a more precise method to isolate the uncorrelated quantum noise from influences such as neuronal activity. This approach is superior to alternative methods that estimate these values over extended time periods, as it better targets the specific characteristics of quantum noise.
6. Plot V against I to create the Photon Transfer Curve.
7. Determine the photon sensitivity q and the zero-intensity level I_0 by performing a linear fit to the photon transfer curve so that $V \approx q \cdot (I - I_0)$. Ensure reliable results by weighing the fit with the pixel count vector C and employing a robust fitting method that minimises the impact of outliers. Our procedure utilised the Huber linear regressor from the *sklearn* package in Python[86].
   ? TROUBLESHOOTING
8. Plot the linear fit alongside the Photon Transfer Curve (see **Fig. 16b**). Look for the characteristic linear portion where photon noise dominates. For static objects, the entire Photon Transfer Curve should align with the linear fit. In dynamic experiments, expect a linear and tight component in darker regions and a quadratic, dispersed component in bright regions.
   ▲ **CRITICAL STEP** The measured photon transfer curve (**Fig. 16b**) reveals a characteristic linear portion at the lower intensity range, indicating the Poissonian properties of the quantum noise. The upper intensity range is dominated by fluorescence signals such as neuronal activity and tissue motion, causing more dispersion with rapidly increasing variance. A robust linear fit (indicated by the red line) isolates the slope of the linear component, the photon sensitivity, with a value of 96.9, signifying that the system digitises images so that 96.9 grayscale levels are used to quantize the average intensity due to one detected photon. The intercept of the linear fit with the x-axis designates the inferred true zero-intensity level.
9. For each pixel in the image, plot the coefficient of variation—the ratio of the pixel's mean value to its variance.
   ▲ **CRITICAL STEP** The coefficient of variation image serves as a diagnostic tool to detect diverse imaging anomalies such as pixel saturations and extra noise sources. Saturated or clipped regions, for instance, will exhibit low coefficients of variation whereas motion, laser fluctuations, and physiological signals will produce high coefficients of variation in the bright regions of the image.

▲ **CRITICAL STEP** Properly scaled by the photon sensitivity, the coefficient equals 1.0 for any Poisson process. In **Fig 16c**, regions with exact Poisson noise prediction appear grey, higher variability regions appear green, and lower-than-expected variance regions appear purple. For instance, green neuronal bodies reflect added variance from neuronal activity, and purplish bands along the frame's edges result from the acquisition system's compensation for slower laser scanning speeds near the boundaries. Since we estimate the average photon sensitivity across the entire image, the method overestimates the photon sensitivity close to edges where the system applies a lower gain. For the same brightness, more photons are detected and less noise results, producing a lower coefficient of variation. This compensation can be undone by using a more accurate local photon sensitivity estimation, although it was not performed here where we estimated the average photon sensitivity for the entire image for simplicity.

10. Rescale the original image sequence as $\hat{X} \leftarrow q \cdot (X - I_0)$ to create photon flux movies where pixel values represent photon flux in units of photon counts per pixel per frame. Alternatively, rescale the images as $\dot{X} \leftarrow q \cdot (X - I_0) / (dx\, dy\, dt)$ for units of photons per square micron per second, where dx and dy denote the pixel pitch in microns, and dt denotes the frame period in seconds.
▲ **CRITICAL STEP** **Fig. 16d** shows several segmented cells detected by thresholding a max projection image across time, subtracting the mean fluorescence. **Fig. 16e** depicts the max projection image across the 500 frames expressed in units of photon flux. Note that the mean photon rates will be significantly lower. The density of intensities shown in **Fig. 16b** indicates that the majority of pixels have intensities on the order of 400, corresponding to (400 – zero level) / sensitivity = 3 photons per pixel per frame in this particular sequence.
11. ▲ **OPTIONAL** Correct the photon flux movie $\hat{X}$ for motion. The pixel interpolations performed by the motion correction algorithm will have a negligible effect on photon rate estimation. Other processing steps, such as temporal or spatial filtrations, might have more complex effects and require careful consideration (not covered here).
12. ▲ **OPTIONAL** For dynamic signals (e.g. calcium imaging), extract the absolute fluorescence signal y by summing pixels over each region of interest R (e.g. a cell) with equal weights:

$$y = \frac{1}{dt} \sum_{i \in R} \hat{X}_i \sum_{i \in R} \hat{X}_i \qquad \text{(eq. 7)}$$

The magnitude of trace y will be correctly expressed in units of photons per second.
13. ▲ **OPTIONAL** The signal y can also be computed using a weighted mask h as:

$$y = \frac{\gamma}{dt} \sum_{i \in R} h_i \hat{X}_i \sum_{i \in R} h_i \hat{X}_i \qquad \text{(eq. 8)}$$

Here γ is the normalisation coefficient for proper scaling of the photon sensitivities. This computation is not trivial for dynamic scenes. The optimal unbiased scaling coefficient is:

$$\gamma = \frac{\sum_{i \in R} h_i \bar{X}_i}{\sum_{i \in R} h_i^2 \bar{X}_i}$$, where $\bar{X}_i$ is the time-averaged pixel value in $\hat{X}_i$.

A simpler normalisation $\gamma = \frac{\sum_{i \in R} h_i}{\sum_{i \in R} h_i^2}$ provides an accurate estimation when the image under the mask is approximately uniform. When the image is non-uniform, then this normalisation results in a lowered estimation. We recommend using this simpler normalisation.
▲ **CRITICAL STEP** Measuring fluorescence in absolute units becomes valuable for monitoring signal quality across various experiments and laboratories. **Fig. 16f** shows the photon rates for the regions of interest (ROIs) corresponding to the detected cells from **Fig. 16d**. Each ROI contains 18-24 pixels with uniform weights.
▲ **CRITICAL STEP** It is important to ensure that no spatial or temporal filtration is applied to the images before the photon rate estimation since it can bias the estimation.
14. Repeat the method on a different system for direct comparison, or on the same system at a later date to track performance.
? TROUBLESHOOTING
▲ **CRITICAL STEP** We applied the same method to a completely different dataset from another lab (**Fig. 17**). This sequence uses a different fluorescent dye, laser setting, optics, and acquisition parameters. Here, the system applies higher gains to compensate for lower pixel dwell times,

producing a photon sensitivity of 678.7 grayscale levels per photon (**Fig. 17a**). While the imaging setups differ substantially, we arrive at comparable magnitudes of the fluorescence signals with peak amplitudes reaching more than 104 photons per second from each cell (**Fig. 17d**).

TROUBLESHOOTING

Procedure	Step	Problem	Possible reason	Possible solution
1	4	Laser power value changes over the course of the day by >5%	If the laser itself is stable, such a change could be due to instability of the power modulator. Pockels cells are temperature sensitive, and a unit with an internal or directly affixed beam dump can drift significantly as the dumped beam could cause strong local heating, especially for lasers with power outputs of a few Watts.	In this case, the beam dump should be decoupled from the Pockels cell, with a short distance between them. CAUTION: beam dump repositioning should only be attempted by a competent, trained, individual. The discarded beam exiting a Pockels cell is of high power and often exits at a dangerous angle, making an eye-strike possible.
1				Similar temperature instabilities can occur if the Pockels cell is downstream of a shutter and only gets the laser beam when imaging is active, as its internal temperature will change as the laser passes through the cell. Open shutters 30-60 minutes before measuring laser power.
1	16	Laser power value changes over the course of minutes and is not stable	Improper use of thermal sensor heads	Thermal power sensors are sensitive to ambient temperature and physical handling, especially at lower power values. The sensor should be allowed to equilibrate and only used once zero drift has ceased. For laser powers under a few mW, users should consider photodiode sensors, as they are less sensitive to external conditions and shielding ambient light is very straightforward, as compared to heat sources.
1	22	Laser power has changed by more than 5% since the first recorded measurem	Laser throughput is changing	Measure laser power directly after the laser enclosure and compare to manufacturer's commissioning values. If the laser power at the laser enclosure has changed by >5%, contact the manufacturer for assistance.

		ent		
1			Laser alignment has changed. Laser power at the objective is highly sensitive to beam alignment. For instance, if the beam is not hitting the scanners correctly, it can be partially clipped, reducing the laser power reaching the sample.	Make a record of the laser power at different points in the beam path to determine if power is being lost. Make logs of these values at the different points along the path after each alignment change to make troubleshooting easier. Useful locations to log transmission would be before and after the modulation device as well as before and after the scan head. Having alignment targets in two or more places on the table and one at the objective mount is also a simple way to troubleshoot if measurements are off due to alignment. If the beam is not hitting the centre of a target, it suggests the laser is misaligned before that point. Adjustable aperture irises are convenient for this purpose, as they can be mounted directly in the path, yet opened for free beam passage under normal conditions. Make a log of laser alignment at apertures and targets to correlate any changes in alignment with changes in laser power.
1			Power sensor has not been calibrated recently	Power sensors may need calibration every 2-3 years, if your values are slowly changing, you may want to recalibrate your power sensor
2	13	Pincushion, barrel distortion and z-plane (field) curvature	Pincushion and barrel distortion are usually caused by optical aberration at high scan angles in excitation optics.	Ideally, the XY beam displacement in the imaging plane depends linearly on the scan angle. Practically, due to optical design compromises, this linearity breaks down at higher scan angles, usually towards the corners of the image. Unfortunately, this is a limitation of the optics and is most easily resolved *post-hoc* by correcting the images. For applications such as functional *in vivo* imaging it may not be necessary to correct for distortion.
3	10	Unusually shaped inhomogeneity that extends along the microscope's fast axis and does not change	One potential source of image inhomogeneity that is not related to the optical properties of the microscope is intensity "ringing" that originates in a Pockels cell (**Fig. 18**). Some	Disabling beam blanking should reduce or eliminate the problem if it originates from the Pockels cell. It is for this reason that we recommend *initial* vignetting measurements are done over a range of zooms. Note that Pockels Cell resonance impacts on inhomogeneity may look different to that shown, as they will depend upon the specifics of how the sample

		shape with zoom	microscopes use an electro-optical power modulator known as a Pockels cell to rapidly control laser power through the application of large voltages to the Pockels cell. The materials used in these cells can have a strong piezo-mechanical effect, resulting in a damped oscillation at the cell's resonance frequency. This is typically seen on the fast scan axis, on Pockels cells that do not have any additional damping (the so-called BK "clamped" option on one common brand, Conoptics).	is imaged, and the nominal scan line duration.
3	14/15	Local inhomogeneities	Bubbles in the immersion media, or inconsistent fluorescence in the imaging sample.	If using a slide, try cleaning it.
3	14/15		Dirt on optics somewhere in the path, it is not unheard of for dust to burn on to optics due to high laser powers.	Try using compressed air to dust the optics in the path to identify if any are causing issues, or where possible directly observe lenses to check for burnt on dust.
3	14/15	Asymmetric drop-off of the fluorescence towards the edges, or off-centre peak	Problems with alignment	This can be confirmed with the measurement of spatial resolution (Procedure 4). The geometry of the excitation volume will most likely be less tight in the area of the FOV that appears darker.
3	14/15	Vignetting	Problems with pupil conjugation in the system	Evaluate whether the beam "walks" at the back pupil.
4	5	Beads move around	Evaporation from the sample being left out too long	Seal the coverslip to the slide if planning to use the slide for a significant amount of time, or if movement of beads is seen.
4	5	Beads appear	Laser power is too high	The use of high power to locate beads may indicate inefficient multiphoton

		damaged, bleach quickly or move around		excitation. For efficient two-photon excitation, a transform-limited pulse in the imaging plane should be used, and thus it is suggested to optimise GDD compensation prior to this protocol (see **Procedure 5**).
4	7	Beads appear damaged, bleach quickly or move around	An overly zoomed-in field-of-view may result in photobleaching and in extreme cases, the excess heat deposited locally could melt the agarose.	Zoom out further while maintaining oversampling (beyond the Nyquist limit) to ensure that the pixel size is still small enough to permit precise curve fitting. If this isn't possible, turn the laser power down.
4	10	Data does not fit a Gaussian curve due to a plateaued peak.	The bead stack has too many saturated pixels.	Operate below the saturation regime to achieve a proper fit and correct estimation of resolution.
4	10	Resulting PSFs are tilted	Optical aberrations tend to increase away from the centre of the field-of-view	One could use a built-in rotation function, such as ImageJ ('Rotate…') and MATLAB ('imrotate'), to correct the tilt in the Gaussian fit.
4	10	Curve fitting is poor	Signal-to-noise ratio is too low for the bead stack	At each z-position in the stack, several frames can be acquired and averaged to yield a higher signal-to-noise image.
5	15	Signal intensity never declines in one direction, but instead, continues to rise until the limit of your dispersion compensation correction is reached.	Not enough dispersion compensation in the system.	Decide to accept the limit GDD value as the "best" correction or consider adding more dispersion through an additional external unit. If the user typically uses a fixed wavelength, multiple bounces between chirped mirrors provides a straightforward way to add dispersion[87].
5	17/18	Fluorescence intensity measurements display sharp peakiness across imaging wavelength	Presence of dielectric mirrors distorting the pulse shape. Complex coatings of dielectric mirrors can have very strong and very specific wavelength dependence of dispersion.	Despite the high reflection efficiencies of multilayer coatings, the authors recommend using metallic mirrors if possible, or dielectric mirrors that are designed and calibrated for known amounts of dispersion. The total effect of dielectric coatings (particularly old ones) on pulse shape cannot be assessed without sophisticated

		s used in experiments (**Fig 19**)		instrumentation, replacing dielectric mirrors with metal-coated alternatives is better than simply "correcting" for GDD peakiness with a pre-chirper[88].
7	7	Nonlinear photon transfer curve	Extremely low photon rates can cause nonlinear PTCs. Our method can produce a nonlinear kink for rates near single photons per frame, complicating sensitivity estimation in dim images.	Increase laser power, dwell time (lower scan speed), detector gain or fluorophore expression.
7	7		Variances growing quadratically with intensity may dominate the PTC in cases of strong fluorescence signals.	Repeat the procedure with a static fluorescent object if needed. However, in multiphoton imaging, we have not encountered such issues even after re-analysing diverse datasets from multiple labs.
7	7		Non-Poissonian noise sources, such as excessive electronic noise or laser fluctuations, can also result in a nonlinear PTC.	These issues should be separately diagnosed and addressed to restore the imaging system to a photon noise-limited state.
7	14	Low photon rates	On occasions, low photon rates, especially in somatic calcium signals, might be expected, particularly in deeper tissue imaging or large fields of view.	Improvements can be achieved by multiple approaches: the incorporation of brighter fluorescent indicators, longer dwell times, increased laser power, optimization of excitation wavelengths, replacement of aged PMTs, or improved beam alignment and the GDD (Group Delay Dispersion) parameters.

● **TIMING**

Procedure 1, measuring laser power at the sample, 2 h
Procedure 2, field of view size, 2 h
Procedure 3, field of view homogeneity, 2 h
Procedure 4, spatial resolution, 3.5 h
Procedure 5, group delay dispersion optimisation, 1.5 h
Procedure 6, photomultiplier tube performance, 3.5 h
Procedure 7, estimating absolute magnitudes of fluorescence signals, 3 h

ANTICIPATED RESULTS

This protocol should be carried out at regular intervals, such as once a month or every 3 months. All

procedures should be repeated after changes are made to laser beam alignment. After installation, alignment can drift due to mirrors settling in place on an optical table. Procedures should be carried out much more frequently towards the start of the microscope system life to ensure a stable baseline is acquired. Frequency will depend on how often the microscope is altered or used; the below recommendations are based on a lab using their system daily for multiple hours. Procedure 1 is expected to change over time due to laser degradation so should be performed once a month, or preferably before every major experiment. Procedure 2 should be carried out once every 6 months to ensure nothing drastic has changed with the system, as it is unlikely that the fundamental properties of the image scale should change on their own. Procedure 3 and 4 should be carried out once every 3 months to ensure consistency. Procedure 5 need only be carried out once every 6 months. Procedure 6 should be carried out monthly to monitor PMT health. Procedure 7 should be carried out once every 6 months and is not essential to monitor performance, but is a good indicator of performance changes.

REFERENCES

1. Goppert-Mayer, M. Elementary file with two quantum fissures. *Ann. Phys.* **9**, 273–294 (1931).

2. Denk, W., Strickler, J. H. & Webb, W. W. Two-photon laser scanning fluorescence microscopy. *Science* **248**, 73–6 (1990).

3. Debarre, D., Olivier, N., Supatto, W. & Beaurepaire, E. Mitigating Phototoxicity during Multiphoton Microscopy of Live Drosophila Embryos in the 1.0-1.2 mu m Wavelength Range. *Plos One* **9**, 12 (2014).

4. Schonle, A. & Hell, S. W. Heating by absorption in the focus of an objective lens. *Opt. Lett.* **23**, 325–327 (1998).

5. Podgorski, K. & Ranganathan, G. Brain heating induced by near-infrared lasers during multiphoton microscopy. *J. Neurophysiol.* **116**, 1012–1023 (2016).

6. Stujenske, J. M., Spellman, T. & Gordon, J. A. Modeling the Spatiotemporal Dynamics of Light and Heat Propagation for In Vivo Optogenetics. *Cell Rep.* **12**, 525–534 (2015).

7. Schmidt, E. & Oheim, M. Infrared Excitation Induces Heating and Calcium Microdomain Hyperactivity in Cortical Astrocytes. *Biophys. J.* **119**, 2153–2165 (2020).

8. Magidson, V. & Khodjakov, A. Circumventing photodamage in live-cell microscopy. *Methods Cell Biol.* **114**, 10.1016/B978-0-12-407761-4.00023–3 (2013).

9. Phototoxicity in live fluorescence microscopy, and how to avoid it - Icha - 2017 - BioEssays - Wiley Online Library. https://onlinelibrary.wiley.com/doi/full/10.1002/bies.201700003.

10. Nadiarnykh, O., Thomas, G., Van Voskuilen, J., Sterenborg, H. & Gerritsen, H. C. Carcinogenic damage to deoxyribonucleic acid is induced by near-infrared laser pulses in multiphoton microscopy via combination of two- and three-photon absorption. *J. Biomed. Opt.* **17**, 7 (2012).

11. Konig, K., Becker, T. W., Fischer, P., Riemann, I. & Halbhuber, K. J. Pulse-length dependence of cellular response to intense near-infrared laser pulses in multiphoton microscopes. *Opt. Lett.* **24**, 113–115 (1999).

12. CFI75 Water Dipping Series. *Nikon Instruments Inc.* https://www.microscope.healthcare.nikon.com/products/optics/cfi75-water-dipping-series.

13. UMPLFLN-W/LUMPLFLN-W/XLUMPLFLN-W/LUMFLN-W | Semi-Apochromat Water Dipping Objectives for Electrophysiology | Olympus LS. https://www.olympus-lifescience.com/en/objectives/lumplfln-w/.

14. Young, M. D., Field, J. J., Sheetz, K. E., Bartels, R. A. & Squier, J. A pragmatic guide to multiphoton microscope design. *Adv. Opt. Photonics* **7**, 276–378 (2015).

15. Smith, S. L. Building a Two-Photon Microscope Is Easy. in *Multiphoton Microscopy* (ed. Hartveit, E.) vol. 148 1–16 (Humana Press Inc, Totowa, 2019).

16. Pawley, J. B. *Handbook of Biological Confocal Microscopy*. (Springer, New York, NY, 2006).

17. *Handbook of Biomedical Nonlinear Optical Microscopy*. (Oxford University Press, Oxford, New York, 2008).

18. Ji, N., Freeman, J. & Smith, S. L. Technologies for imaging neural activity in large volumes. *Nat.*

Neurosci. **19**, 1154–1164 (2016).

19. Zinter, J. P. & Levene, M. J. Maximizing fluorescence collection efficiency in multiphoton microscopy. *Opt. Express* **19**, 15348–15362 (2011).

20. Bumstead, J. R. *et al.* Designing a large field-of-view two-photon microscope using optical invariant analysis. *Neurophotonics* **5**, 025001 (2018).

21. Zipfel, W. R., Williams, R. M. & Webb, W. W. Nonlinear magic: Multiphoton microscopy in the biosciences. *Nat. Biotechnol.* **21**, 1369–1377 (2003).

22. Heintzmann, R. & Sheppard, C. J. R. The sampling limit in fluorescence microscopy. *Micron* **38**, 145–149 (2007).

23. Lu, R. W. *et al.* Video-rate volumetric functional imaging of the brain at synaptic resolution. *Nat. Neurosci.* **20**, 620-+ (2017).

24. Quirin, S., Peterka, D. S. & Yuste, R. Instantaneous three-dimensional sensing using spatial light modulator illumination with extended depth of field imaging. *Opt. Express* **21**, 16007–16021 (2013).

25. Weisenburger, S. *et al.* Volumetric Ca2+ Imaging in the Mouse Brain Using Hybrid Multiplexed Sculpted Light Microscopy. *Cell* **177**, 1050-+ (2019).

26. Song, A. *et al.* Volumetric two-photon imaging of neurons using stereoscopy (vTwINS). *Nat. Methods* **14**, 420-+ (2017).

27. Tan, X. J. *et al.* Volumetric two-photon microscopy with a non-diffracting Airy beam. *Opt. Lett.* **44**, 391–394 (2019).

28. Yang, W. *et al.* Simultaneous Multi-plane Imaging of Neural Circuits. *Neuron* **89**, 269–84 (2016).

29. Helmchen, F. & Denk, W. Deep tissue two-photon microscopy. *Nat. Methods* **2**, 932–940 (2005).

30. Gobel, W. & Helmchen, F. In vivo calcium Imaging of neural network function. *Physiology* **22**, 358–365 (2007).

31. Sherman, L., Ye, J. Y., Albert, O. & Norris, T. B. Adaptive correction of depth-induced aberrations in multiphoton scanning microscopy using a deformable mirror. *J. Microsc.* **206**, 65–71 (2002).

32. Turcotte, R., Liang, Y. J. & Ji, N. Adaptive optical versus spherical aberration corrections for in vivo brain imaging. *Biomed. Opt. Express* **8**, 3891–3902 (2017).

33. Visser, T. D. & Oud, J. L. VOLUME MEASUREMENTS IN 3-DIMENSIONAL MICROSCOPY. *Scanning* **16**, 198–200 (1994).

34. Diel, E. E., Lichtman, J. W. & Richardson, D. S. Tutorial: avoiding and correcting sample-induced spherical aberration artifacts in 3D fluorescence microscopy. *Nat. Protoc.* **15**, 2773–2784 (2020).

35. Wang, K., Liang, R. F. & Qiu, P. Fluorescence Signal Generation Optimization by Optimal Filling of the High Numerical Aperture Objective Lens for High-Order Deep-Tissue Multiphoton Fluorescence Microscopy. *Ieee Photonics J.* **7**, 8 (2015).

36. Takasaki, K., Abbasi-Asl, R. & Waters, J. Superficial Bound of the Depth Limit of Two-Photon Imaging in Mouse Brain. *Eneuro* **7**, 10 (2020).

37. Kondo, M., Kobayashi, K., Ohkura, M., Nakai, J. & Matsuzaki, M. Two-photon calcium imaging of the medial prefrontal cortex and hippocampus without cortical invasion. *eLife* **6**, e26839 (2017).

38. Yamaguchi, K., Kitamura, R., Kawakami, R., Otomo, K. & Nemoto, T. In vivo two-photon microscopic observation and ablation in deeper brain regions realized by modifications of excitation beam diameter and immersion liquid. *PLoS ONE* **15**, e0237230 (2020).

39. Hampson, K. M. *et al.* Adaptive optics for high-resolution imaging. *Nat. Rev. Methods Primer* **1**, 26 (2021).

40. Hirlimann, C. *Femtosecond Laser Pulses: Principles and Experiments*. vol. Advanced texts in physics (Springer, 2005).

41. Dispersion (optics). *Wikipedia* (2023).

42. Sofroniew, N. J., Flickinger, D., King, J. & Svoboda, K. A large field of view two-photon mesoscope with subcellular resolution for in vivo imaging. *Elife* **5**, 20 (2016).

43. Tai, S.-P. *et al.* Two-photon fluorescence microscope with a hollow-core photonic crystal fiber. *Opt. Express* **12**, 6122–6128 (2004).

44. Zong, W. *et al.* Fast high-resolution miniature two-photon microscopy for brain imaging in freely behaving mice. *Nat. Methods* **14**, 713–719 (2017).

45. Farinella, D. M., Roy, A., Liu, C. J. & Kara, P. Improving laser standards for three-photon microscopy. *Neurophotonics* **8**, 015009 (2021).

46. Borzsonyi, A., Kovacs, A. P. & Osvay, K. What We Can Learn about Ultrashort Pulses by Linear Optical Methods. *Appl. Sci.* **3**, 515–544 (2013).

47. Hamamatsu Photonics KK. *Photomultiplier Tubes: Basics and Applications*. (Hamamatsu Photonics K.K., 2017).

48. Wang, T. *et al.* Quantitative analysis of 1300-nm three-photon calcium imaging in the mouse brain. *eLife* **9**, e53205 (2020).

49. Samei, E. Performance of Digital Radiographic Detectors: Quantification and Assessment Methods. *RSNA Categ. Course Diagn. Radiol. Phys.* 37–47 (2003).

50. Measuring the gain of your imaging system – Labrigger. https://labrigger.com/blog/2010/07/30/measuring-the-gain-of-your-imaging-system/.

51. Huang, L. *et al.* Relationship between simultaneously recorded spiking activity and fluorescence signal in GCaMP6 transgenic mice. *eLife* **10**, e51675 (2021).

52. Lecoq, J., Orlova, N. & Grewe, B. F. Wide. Fast. Deep: Recent Advances in Multiphoton Microscopy of *In Vivo* Neuronal Activity. *J. Neurosci.* **39**, 9042–9052 (2019).

53. In Vivo Optical Imaging of Brain Function, Second Edition. in *In Vivo Optical Imaging of Brain Function, Second Edition* (ed. Frostig, R. D.) 1–472 (Crc Press-Taylor & Francis Group, Boca Raton, 2009). doi:10.1201/9781420076851.

54. Rosenegger, D. G., Tran, C. H. T., Ledue, J., Zhou, N. & Gordon, G. R. A High Performance, Cost-Effective, Open-Source Microscope for Scanning Two-Photon Microscopy that Is Modular and Readily

Adaptable. *Plos One* **9**, 16 (2014).

55. Mayrhofer, J. M. *et al.* Design and performance of an ultra-flexible two-photon microscope for in vivo research. *Biomed. Opt. Express* **6**, 4228–4237 (2015).

56. Corbin, K., Pinkard, H., Peck, S., Beemiller, P. & Krummel, M. F. Chapter 8 - Assessing and benchmarking multiphoton microscopes for biologists. in *Methods in Cell Biology* (eds. Waters, J. C. & Wittman, T.) vol. 123 135–151 (Academic Press, 2014).

57. Diaspro, A., Chirico, G. & Collini, M. Two-photon fluorescence excitation and related techniques in biological microscopy. *Q. Rev. Biophys.* **38**, 97–166 (2005).

58. Kerr, J. N. D. & Denk, W. Imaging in vivo: watching the brain in action. *Nat. Rev. Neurosci.* **9**, 195–205 (2008).

59. So, P. T. C., Dong, C. Y., Masters, B. R. & Berland, K. M. Two-photon excitation fluorescence microscopy. *Annu. Rev. Biomed. Eng.* **2**, 399–429 (2000).

60. Mostany, R., Miquelajauregui, A., Shtrahman, M. & Portera-Cailliau, C. Two-Photon Excitation Microscopy and Its Applications in Neuroscience. in *Advanced Fluorescence Microscopy: Methods and Protocols* (ed. Verveer, P. J.) vol. 1251 25–42 (Humana Press Inc, Totowa, 2015).

61. Negrean, A. & Mansvelder, H. D. Optimal lens design and use in laser-scanning microscopy. *Biomed. Opt. Express* **5**, 1588–1609 (2014).

62. Gaudreault, N. *et al.* Illumination Power and illumination stability. (2022).

63. Nelson, G. *et al.* Monitoring the point spread function for quality control of confocal microscopes. (2022).

64. Faklaris, O. *et al.* Quality assessment in light microscopy for routine use through simple tools and robust metrics. *J. Cell Biol.* **221**, e202107093 (2022).

65. Cole, R. W., Jinadasa, T. & Brown, C. M. Measuring and interpreting point spread functions to determine confocal microscope resolution and ensure quality control. *Nat. Protoc.* **6**, 1929–1941 (2011).

66. Jonkman, J., Brown, C. M., Wright, G. D., Anderson, K. I. & North, A. J. Tutorial: guidance for quantitative confocal microscopy. *Nat. Protoc.* **15**, 1585–1611 (2020).

67. Llopis, P. M. *et al.* Best practices and tools for reporting reproducible fluorescence microscopy methods. *Nat. Methods* **18**, 1463-+ (2021).

68. Demmerle, J. *et al.* Strategic and practical guidelines for successful structured illumination microscopy. *Nat. Protoc.* **12**, 988–1010 (2017).

69. Saidi, S. & Shtrahman, M. Evaluation of compact pulsed lasers for two-photon microscopy using a simple method for measuring two-photon excitation efficiency. *Neurophotonics* **10**, 044303 (2023).

70. Stack, R. F. *et al.* Quality Assurance Testing for Modern Optical Imaging Systems. *Microsc. Microanal.* **17**, 598–606 (2011).

71. Tang, S., Krasieva, T. B., Chen, Z., Tempea, G. & Tromberg, B. J. Effect of pulse duration on two-photon excited fluorescence and second harmonic generation in nonlinear optical microscopy. *J. Biomed. Opt.* **11**, 3 (2006).

72. SWC-Advanced-Microscopy/measurePSF. SWC Advanced Microscopy Facility (2024).

73. Distortion (optics). *Wikipedia* (2023).

74. Stirman, J. N., Smith, I. T., Kudenov, M. W. & Smith, S. L. Wide field-of-view, multi-region, two-photon imaging of neuronal activity in the mammalian brain. *Nat. Biotechnol.* **34**, 857-+ (2016).

75. Tsai, P. S. *et al.* Ultra-large field-of-view two-photon microscopy. *Opt. Express* **23**, 13833–13847 (2015).

76. Pogue, B. W. & Patterson, M. S. Review of tissue simulating phantoms for optical spectroscopy, imaging and dosimetry. *J. Biomed. Opt.* **11**, 16 (2006).

77. fmi-faim/napari-psf-analysis. FAIM (2024).

78. Kane, S. & Squier, J. Grism-pair stretcher-compressor system for simultaneous second- and third-order dispersion compensation in chirped-pulse amplification. *J. Opt. Soc. Am. B-Opt. Phys.* **14**, 661–665 (1997).

79. Chauhan, V., Bowlan, P., Cohen, J. & Trebino, R. Single-diffraction-grating and grism pulse compressors. *J. Opt. Soc. Am. B-Opt. Phys.* **27**, 619–624 (2010).

80. Yakovlev, I. V. Stretchers and compressors for ultra-high power laser systems. *Quantum Electron.* **44**, 393 (2014).

81. McFadden, D., Amos, B. & Heintzmann, R. Quality Control of Image Sensors using Gaseous Tritium Light Sources. *Philos. Transact. A Math. Phys. Eng. Sci.* **380**, 20210130 (2022).

82. Tritium radioluminescence. *Wikipedia* (2023).

83. Janesick, J. R. *Photon Transfer : DN [Lambda]*. (SPIE Bellingham, Wash., Bellingham, Wash., 2007).

84. Consortium, T. Mic. *et al.* Functional connectomics spanning multiple areas of mouse visual cortex. 2021.07.28.454025 Preprint at https://doi.org/10.1101/2021.07.28.454025 (2023).

85. 000402/0.230307.2132 - DANDI Archive. https://dandiarchive.org/dandiset/search?search=000402%2F0.230307.2132.

86. Pedregosa, F. *et al.* Scikit-learn: Machine Learning in Python. *J. Mach. Learn. Res.* **12**, 2825–2830 (2011).

87. Keller, U. *Ultrafast Lasers: A Comprehensive Introduction to Fundamental Principles with Practical Applications*. (Springer International Publishing, Cham, 2021). doi:10.1007/978-3-030-82532-4.

88. Rupprecht, P. Pulse dispersion, dielectric mirrors and fluorescence yield: A case report of a two-photon microscope. *Github.io* (2019).

ACKNOWLEDGEMENTS

This research was funded in part by the Wellcome Trust [204651/Z/16/Z, 220273/Z/20/Z]. For the purpose of Open Access, the author has applied a CC BY public copyright licence to any Author Accepted Manuscript version arising from this submission. This work was also supported by funding from the European Research Council (ERC) under the European Union's Horizon 2020 research and innovation program (grant agreement No 852765), the National Institutes of Health (R01EY035378 and RF1NS121919 to S.L.S., U24NS116470 to D.Y., U19NS104649 and U01NS113273 to D.S.P.), and the National Science Foundation (1934288 to S.L.S.).

AUTHOR CONTRIBUTIONS

Investigation: **All authors**

Writing – original draft:

- Laser Power at the Sample: **R.M.L., R.A.A.C., N.O.**
- Field of View Size: **R.A.A.C., N.O.**
- Field of View Homogeneity: **R.A.A.C., N.O., R.M.L.**
- Spatial Resolution: **S.L.S., C-H.Y.**
- Pulse Width Control and Optimisation: **D.S.P, R.A.A.C.**
- Photomultiplier Tube Performance: **I.H.B., B.P.**
- Estimating Absolute Magnitudes of Fluorescence Signals: **D.Y.**

Writing – review & editing: **All authors**

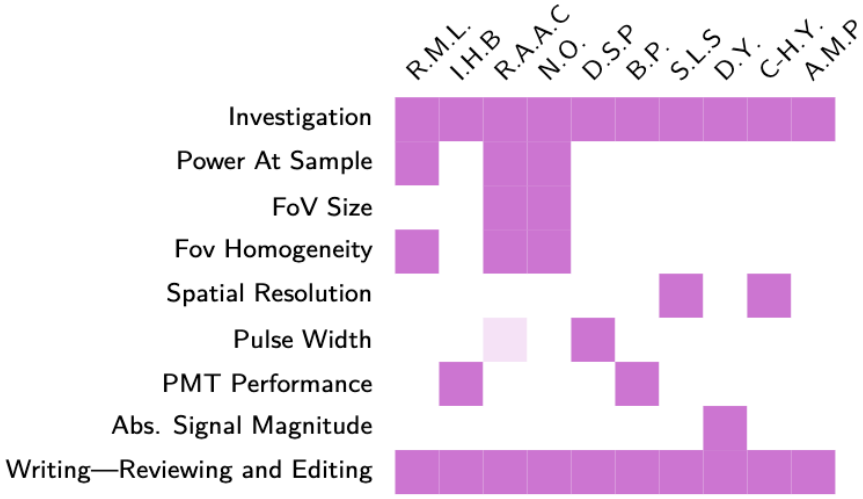

COMPETING INTERESTS

TheThe authors declare no competing interests.

FIGURE LEGENDS

Figure 1. Basic schematic of a resonant-scanning multiphoton microscope.

Figure 2. **Object distortion caused by refractive index mismatching and the correction factor** (modified from Fig. 2d in [34]). **a.** Scanning the objective lens axially (indicated by the black arrow, Δ objective) through a spherical object (labelled as the "actual object" in purple, Δ focus) submerged in water produces a 3D image. Despite this, the image (labelled as the "apparent object" in green) appears compressed along the axial direction. This compression arises due to the air-to-water interface, where the refractive index transitions from air ($RI_{IMMERSION}$ = 1) to water (RI_{SAMPLE} = 1.33), causing light rays (purple rays) to bend. Consequently, the movement of the objective (Δ objective) is smaller than that of the actual focal plane (Δ focus). The resulting rendering of the sphere ('apparent object', green) exhibits axial compression, as the acquisition software assigns the objective's travel distance (Δ objective) rather than the focal plane's travel distance (Δ focus) to the object's z-axis. A correction factor can be calculated and applied to correct this distortion. (B) A plot shows the correction factor converting the movement of the objective (Δobjective) or the z-stage (Δstage) to that of the actual imaging plane (Δfocus) as a function of NA of the objective. $RI_{IMMERSION} = n_1 = 1$, and $RI_{SAMPLE} = n_2 = 1.33$.

Figure 3. Laser power measurement. a. The path of a resonant-scanned focused laser beam over a sample. The beam moves sinusoidally along the fast axis (X in this case) whilst being scanned in orthogonal Y direction with a linear galvo. The area over which the beam moves is known as the scan field. On the left and right edges the beam slows as the scanner changes direction and turns around. In these areas the potential for photodamage is greatest, as the beam is travelling more slowly over the sample. Thus the beam is typically "blanked" or disabled during these epochs. In a resonant scanning microscope the beam is usually blanked about 30% of the time. The image field (red lines and grey region) is the area over which the beam is on and capable of exciting fluorescence. The dotted lines indicate the blanked turn-around regions. A power meter cannot distinguish these states and so returns aa time-averaged power value over the whole scan field if the microscope is scanning during a measurement. **b**. Position of the power meter head with respect to the laser beam exiting the objective. The sensor surface should be close but must not be at the working distance of the objective lens, as the focussed beam may damage the sensor surface leading to unreliable measurements and permanent damage to the sensor. **c.** Example laser power calibration curve. Output power can be represented as a percentage of total available laser power, or in direct power units, mW, depending on microscope configuration. The purpose is to create a lookup table that allows linear adjustment of power on the edges of the modulation range for modulation devices (like Pockels cells) that have nonlinear response.

Figure 4. Field of view size measurement. a. Two-photon image of a 1 mm grid with 100 µm divisions for the maximum scan angle of the microscope system (i.e. the minimum zoom). Here, the FOV size is ~800 µm. b**.** Image of a 25 µm copper EM grid. This image shows the ~1200 µm FOV and displays minor pincushion distortion at the left and right edges (note how the vertical line on the right and left sides bows in from the vertical line defined by the edge of the image). **c**. Grid lines are detected and overlaid on top of the EM grid image using the "MicsPerPixel" software tool[72].

Figure 5. Field of view size comparison for two-photon and epifluorescent modes on a large field of view microscope (Mesoscope). a. Tiled two-photon image of the Mesoscope FOV (~5000 µm). **b.** Epifluorescent image of the Mesoscope FOV showing a ~45 degree rotation, and vertical reflection, compared to the two-photon image.

Figure 6. Field of view homogeneity. a. Homogeneity calibration image of the uniform fluorescent slide acquired using a 16x objective at maximum scan angle on a system that allows for large scan angles. Homogeneity drop-off profiles and different zoom factor overlays are shown (different systems may have different scan areas for the corresponding "zoom" factor). The area of peak brightness is offset downwards slightly in the y-axis. This indicates a possible misalignment in the optics. Dark spots arise from imperfections in the slide surface. **b**. Intensity profiles along horizontal (red) and vertical (cyan) axis demonstrate non-uniformity of excitation at the maximum zoom factor.

Figure 7. **Two-photon full-width at half-maximum (FWHM) as a function of numerical aperture (NA) and wavelengths.** The formula is adapted from Zipfel et al. 2003[21]. NA is the numerical aperture of the objective lens. In FWHMz, n is the refractive index of the medium where the sample is embedded, and set as water in this plot. The refractive index of the water, n, is wavelength dependent, and is [1.328, 1.3255, 1.3225] at [0.9, 1.1, 1.3] µm, respectively.

Figure 8. Example measurement of point spread functions (PSFs). 0.2 µm fluorescent beads were embedded in 0.75% (wt/vol) agarose gel. 40 µm z-stacks were acquired at the depth of 500 µm. Beads at the centre (**a**) and the edge (**b**) of the field-of-view were measured. The example images are shown from the XY, XZ, and YZ cross-sections, respectively. The intensity profiles of the beads (red lines) in the X direction on the XY plane and in the Z direction are plotted, which are fitted to a Gaussian curve (orange dashed line) to extract the radial-X and axial FWHM of the PSF. Note PSF degradation for lateral position of the bead.

Figure 9. Example image pixel histogram. The pixel intensity value distribution is shown for one image frame while live scanning. The spread of this distribution is used to optimise laser pulse width.

Figure 10. Pulse width optimisation measurement. a. Plot of mean image intensity versus GDD compensation value for a fixed average laser power. For this system, around -12000 fs^2 of compensation is necessary for the microscope to achieve highest excitation efficiency. **b**. Example images acquired of the different settings of GDD compensator, and projected intensity plots that can be used for analysis described in the procedure.

Figure 11. **A hand-made tritium light source**. **a.** 3 x 11 mm tritium vial next to a 5 cents coin. **b**. The assembled tritium light source. The pinhole is at the top and will be placed immediately beneath the objective to test the entire collection system, or PMT window to

directly test the PMT. **c**. The multicolour assortment of tritium capsules, each with a different colour phosphor. Shown without a pinhole for clarity. SM1A6 Thorlabs parts were used here for a specific setup, which is not part of this procedure.

Figure 12. First-day performance for three multialkali PMT units of the same model. Mean pixel value (**a**), SNR (**b**), ROC-AUC (**c**) and mean Anode Current (**d**) data shown for three Hamamatsu R10699 PMTs on the first day of installation. PMTs were tested within the full collection optics system (green channel) of the same microscope. Gain setting is represented by the control signal voltage.

Figure 13. Change in PMT performance over time. Mean pixel value (**a**), SNR (**b**), ROC-AUC (**c**) and mean Anode Current (**d**) collected for a Hamamatsu R10699 PMT unit when it was first installed and after 1.5 years of routine use. Dashed line shows pixel values expected based upon tritium decay alone. Gain setting is represented by the control signal voltage.

Figure 14. Pixel grayscale value distributions and ROC-AUC at a series of gain settings for an example multialkali PMT. For each gain setting, distributions of pixel values from dark response (black) and light response (red) images are shown. Corresponding ROC-AUC values are indicated at the top of each panel. Gain expressed as control signal voltage [mV].

Figure 15. Comparison of two different GaAsP PMTs of the same model (Hamamatsu H10770PB-40). Mean (row 1), standard deviation (row 2), ROC-AUC (row 3) and SNR (row 4) for two example GaAsP PMTs for two different tritium light sources (red & green) and control (no light source). PMTs were measured with bandpass filters in place (PMT1: 570-620 nm bandpass; PMT2: 500-550 nm bandpass).

Figure 16. **Photon transfer analysis. a.** The average image of a 500-frame two-photon calcium imaging sequence in mouse visual cortex recorded at 8 frames per second. **b.** The Photon Transfer Curve computed from the same sequence. It features a long linear portion corresponding to Poissonian noise dominating the frame-to-frame variance in all but the brightest regions. The slope of the robust linear fit (red line) reveals the photon sensitivity of 96.9 grayscale levels per photon. Note that the density of intensity values follows a long-tail distribution. The variance in bright regions of the image grows faster than predicted by the linear fit, reflecting the presence of physiological signals. Static images lack such deviations. **c.** The Coefficient of Variation (CoV) image reveals areas of higher variance than predicted from quantum noise alone. Calcium activity in cells produces a higher CoV, shading them green. **d.** Cell segmentation based on the max projection image; eight cells are delineated. **e.** The maximum photon flux per pixel expressed in the units of photons per pixel per frame. **f.** The fluorescence traces from the labelled cells expressed as photons per second. The scale bar on top measures 10^4 photons per second per cell.

Figure 17. A different image sequence from another source. **a.** The Photon Transfer Curve indicates that most pixels don't see a photon in each frame. The PTC has a non-Poissonian segment where no photons are detected. **b.** The Coefficient of Variation image reveals no deviations from predicted variance. **c.** The maximum photon flux is substantially lower than in our first dataset, due to the finer pixel pitch. However, the number of pixels per cell is about 4 times larger. **d.** After ROI averaging, fluorescence signals produced comparable peak amplitudes to the first data set.

Figure 18. Pockels Cell resonance effect. a. Image of a homogeneous fluorescent medium with no ringing effect. **b**. Line profile along the yellow line in **a** that only shows a drop at the dark spot along the line. **c**. Same image as **a**, but with Pockels cell ringing visible on the left side. **d**. Line profile along yellow line in **c** that shows intensity oscillations on the left side of the image where Pockels cell ringing is present. This effect does not change with zoom factor. The line profile is chosen to extend over a darker spot to highlight the magnitude of the ringing.

Figure 19. The effect of dielectric coatings on GDD. Optimal GDD was estimated using a fluorescent slide and the built-in GDD compensation on a Coherent Chameleon Vision II laser. The compensation curve was first measured with three dielectric coated mirrors (ThorLabs EO3) in the path (black line). Obvious sharp peakiness is seen in the required compensation value as a function of wavelength. After these three mirrors were swapped with metallic coated mirrors, the peakiness completely disappears (red line). The three EO3 mirrors did not contribute equally to the above effect (data not shown).